ST Boyle, WV Ingman, V Poltavets, JW Faulkner, RJ Whitfield, SR McColl, and M Kochetkova

The chemokine receptor CCR7 promotes mammary tumorigenesis through amplification of stem-like cells

Oncogene, 2016; 35(1):105-115

Final publication at http://dx.doi.org/10.1038/onc.2015.66

The chemokine receptor CCR7 promotes mammary tumourigenesis through amplification of stem-like cells

Sarah T. Boyle[1], Wendy V. Ingman[2],Valentina Poltavets[1], Jessica W. Faulkner[1], Robert J. Whitfield[3], Shaun R. McColl[1,4], Marina Kochetkova[1]

[1]Discipline of Microbiology and Immunology, School of Molecular and Biomedical Science, University of Adelaide, Adelaide, South Australia, Australia

[2]The Robinson Institute, University of Adelaide, Adelaide, South Australia, Australia; and Discipline of Surgery, School of Medicine, The Queen Elizabeth Hospital, University of Adelaide, Adelaide, South Australia, Australia

[3]Breast, Endocrine and Surgical Oncology Unit, Royal Adelaide Hospital, Adelaide, South Australia, Australia; and Clinical Associate Lecturer, School of Medicine, University of Adelaide, Adelaide, South Australia, Australia

[4]Centre for Molecular Pathology, University of Adelaide, Adelaide, South Australia, Australia

CORRESPONDING AUTHOR:

Dr. Marina Kochetkova

School of Molecular and Biomedical Science

University of Adelaide, Adelaide, SA 5005

E-mail: marina.kochetkova@adelaide.edu.au

Tel: (08) 8313 4553 Fax: 0 8313 4362

RUNNING TITLE: CCR7 promotes breast cancer via stem-like cells

WORD COUNT: 4,700

NUMBER OF FIGURES: 6

ABSTRACT

The chemokine receptor CCR7 is widely implicated in breast cancer pathobiology. Although recent reports correlated high CCR7 levels with more advanced tumor grade and poor prognosis, limited *in vivo* data is available regarding its specific function in mammary gland neoplasia and the underlying mechanisms involved. To address these questions we generated a MMTV-PyMT *Ccr7*$^{-/-}$ bigenic mouse breast cancer model which revealed that CCR7 ablation results in a considerable delay in tumor onset as well as significantly reduced tumor burden. Importantly, CCR7 was found to exert its function by regulating mammary cancer stem-like cells in both murine and human tumors. *In vivo* experiments showed that loss of CCR7 activity either through deletion or pharmacological antagonism significantly decreased functional pools of stem-like cells in mouse primary mammary tumors, providing a mechanistic explanation for the tumor-promoting role of this chemokine receptor. These data characterize the oncogenic properties of CCR7 in mammary epithelial neoplasia and point to a new route for therapeutic intervention to target evasive cancer stem cells.

KEYWORDS: Mammary Gland; Breast Cancer; Cancer Stem Cells; Chemokine Receptors; CCR7; Transgenic Mouse Model

INTRODUCTION

Despite concerted efforts and significant advances, breast cancer-related mortality is still a leading cause of death in women worldwide (1). Clearly novel therapies are urgently needed. The "cancer stem cell" theory specifies that a small subset of cells in a heterogeneous tumor (termed "cancer stem cells" (CSCs)) possess stem cell-like properties of self-renewal and differentiation. CSCs are suggested to sustain and propagate tumors, and are inherently therapy-resistant (for the latest reviews see (2) and (3)).

CSCs may originate from adult stem cells, but can also arise from more committed lineage progenitor cells if they acquire stem cell-like features due to genetic or epigenetic changes (4). Multiple intrinsic and extrinsic factors are reported to play a role in CSC maintenance, regulation and support of stem-like characteristics. Most prominent are the Notch (5), Hedgehog (6), Wnt (7) and TGFβ (8) signaling systems. Several cytokines and chemokines have been recently suggested as maintaining and promoting the CSC phenotype in a number of solid malignancies, including mammary tumors (reviewed in (9)), however, definitive *in vivo* data has been sparse.

Chemokine receptors and their cognate chemokine ligands have become widely accepted as important mediators of cancer growth and progression in many human neoplasms, being involved in tissue transformation, invasion, angiogenesis, and resistance to chemotherapy (10). Amongst these, the chemokine receptor CCR7 has been implicated in metastatic spread of multiple malignancies (11). In breast carcinogenesis it has been attributed a number of potential functions, including promotion of cell motility, migration and adhesion, regulation of matrix metalloproteinases leading to basement membrane degradation (12), and cell survival through inhibition of anoikis (13). Data obtained using cell lines has implicated CCR7 in breast cancer spread to the lymph nodes (14), and in human breast cancer its role was inferred from retrospective studies on archived tumor tissues (15). High

expression levels of CCR7 were also correlated with higher grade and occurrence of secondary tumors, and poor prognosis (16, 17).

Whilst all these studies point to a role for CCR7 in malignancy, a direct function for CCR7 in cancer has not yet been established. Furthermore, its role in breast cancer in particular is unclear. We show here the development of a novel bigenic mouse model combining deletion of CCR7 with the polyoma middle-T transgene, which is under control of the mouse mammary tumor virus promoter (MMTV-PyMT), to study tumor development *in vivo*. Using this model we show that CCR7 deletion has a striking preventative effect on PyMT-driven mammary tumors, supporting the notion that CCR7 plays a major determining role in breast oncogenesis. Moreover, our data reveal that the tumor-promoting effect of CCR7 is mediated through stem-like cells in both primary mouse and human breast tumors. These results provide new insights into the role of CCR7 in breast cancer stem-like cells and have important implications for the development of future therapeutics in breast cancer.

RESULTS

CCR7 deletion arrests mammary tumourigenesis in the PyMT transgenic breast cancer mouse model

The MMTV-PyMT transgenic breast cancer mouse model has been extensively used in recent years to study various aspects of mammary neoplasia. Expression of the PyMT protein promotes the rapid epithelial transformation of mammary cells, via the corruption of various pathways including those of *Src*, *ras*, and PI3 kinase. This model also results in spontaneous metastasis and has been found to closely mimic the development of human breast cancer (18-20). Representative images are shown in Supplementary Figure 1a, in which α-smooth muscle actin (α-SMA) is used to stain myoepithelial cells.

To directly assess the role of CCR7 in the multistage process of mammary tumourigenesis *in vivo*, we generated bigenic MMTV-PyMT *Ccr7*$^{-/-}$ knock-out mice (further referred to as CCR7 KO+) and traced the development of mammary tumors relative to MMTV-PyMT *Ccr7*^{WT} mice (further referred to as WT+).

Deletion of CCR7 significantly delayed PyMT-driven primary mammary tumourigenesis (representative pictures Figure 1a). Tumor-free survival was significantly extended (Figure 1b) and total tumor burden was markedly reduced in CCR7 KO+ mice (Figure 1c) when compared to the WT+ animals. The lungs of WT+ and CCR7 KO+ females were also examined for metastatic lesions at the time of sacrifice. CCR7 KO+ mice developed significantly fewer and smaller metastases than WT+ mice (Figure 1d-f), although, the number of metastases varied largely between mice of the same genotype.

As these experiments indicated a role for CCR7 in mammary gland function, we next examined normal, pre-cancerous and cancer-bearing mouse mammary glands for CCR7 expression and signaling. CCR7 was shown to be expressed on all mouse mammary epithelial cells tested regardless of the tumor stage (Supplementary Figure 1b), and the removal of

CCR7 did not affect the expression levels of its ligands CCL19 and CCL21 within the mouse fat pad (Supplementary Figure 2a). CCR7 was also found to be functional in PyMT-driven mammary tumors, as tumor cells mobilized intracellular calcium, a hallmark of chemokine receptor activity, in response to stimulation with CCL21 (Supplementary Figure 2b). These data showed that CCR7 was expressed and was functional within normal and transformed mammary epithelium.

Interestingly, despite the large impact of CCR7 on overall mammary tumourigenesis, initial PyMT-driven hyperplastic growth in 8 or 11 week old WT+ and CCR7 KO+ mice was not affected (Supplementary Figure 3a), with similar tissue architecture in glands from both genotypes (Supplementary Figure 3b). This indicated that the CCR7 KO+ mammary glands underwent the initial oncogenic transformation leading to epithelial proliferation, but further tumourigenic transition was largely blocked by CCR7 deletion.

CCR7 promotes tumourigenesis by amplifying breast cancer stem-like cells

In order to investigate the underlying mechanisms responsible for the tumourigenic effects seen, we examined the roles of CCR7 in mammary gland development and on stem-like cells. We found that in non-PyMT wild-type (WT) pubertal mice, the epithelial tree was longer with a better developed ductal structure than that in *Ccr7*$^{-/-}$ (CCR7 KO) mice (Figure 2a-b), indicating that ablation of CCR7 had a mild inhibitory effect on pubertal growth of the mammary gland epithelium. CCR7 was robustly expressed in normal mammary epithelium (Figure 2c), making this receptor also potentially relevant to normal mammary development. However, development of mammary epithelium in the CCR7 KO mice caught up with that of the WT mice by the age of 8 weeks, and at 12 weeks mammary glands from the two genotypes were indistinguishable (Figure 2d), demonstrating that CCR7 deletion mainly delays early mammary gland development.

Because normal development and breast cancer are believed to be linked by common regulatory mechanisms, we hypothesized that the observed promotion of PyMT-driven tumourigenesis and mammary development was due to CCR7 regulating stem/progenitor cell pools in mammary epithelium. Thus we next assayed the stem-like cell content in mice using the lineage-negative (Lin^-) $CD24^+CD29^{hi}$ cell surface marker profile (4), which was previously functionally characterized in the MMTV-PyMT model (21, 22). CCR7 was expressed in all cell lineages in both the normal and PyMT-expressing mammary glands regardless of CD24 and CD29 status. Notably however, higher levels of CCR7 (>90%) were observed in $Lin^-CD24^+CD29^{hi}$ normal and cancer mouse mammary stem cell-enriched populations (Figure 3a, Supplementary Figure 4a-b). Importantly, CCR7 was also expressed on human $CD44^+CD24^-$ putative mammary stem cells (23) from both normal and breast tumor tissue (Figure 3b, Supplementary Figure 4c).

Further analysis demonstrated a significantly lower content of $Lin^-CD24^+CD29^{hi}$ cells in non-PyMT CCR7 KO mice relative to WT (Figure 3c left panel). In PyMT-expressing mice at the stage of early neoplasia, when no morphological differences were found in WT+ and CCR7 KO+ glands (Supplementary Figure 3) and the stem/progenitor cell populations may therefore best reflect the tumor-initiating cell content, the difference in the stem cell-enriched population between WT+ and CCR7 KO+ mice was even more pronounced with the deletion of CCR7 leading to a 2-fold reduction in stem-like cells (Figure 3c right panel).

Recently Pece *et al* have suggested a new and potentially more efficient set of markers, in which the Notch ligands Delta-Like Ligand 1 (DLL1) and Delta and Notch-like Epidermal growth factor-related Receptor (DNER) are used in combination with CD49f ($Lin^-CD49f^+DLL1^+DNER^+$) to delineate putative stem cells in human mammary tumors (24). We found that the stem-like cells from both human and mouse mammary glands defined by this profile also expressed high levels of CCR7 (Supplementary Figure 4d-e). Moreover, the Lin^-

$CD49f^{+}DLL1^{+}DNER^{+}$ cell pools were significantly smaller in both normal and PyMT-expressing CCR7 KO murine mammary glands (Supplementary Figure 5a-b) providing further support for the findings described above.

It is generally accepted that non-adherent passaged mammosphere cultures are enriched in cells with stem-like characteristics, and secondary/tertiary mammosphere-forming efficiency (MFE) is representative of cells' potential to exhibit stem cell traits (25-27). Stem-like activity, as measured by MFE, was then analyzed in the mammary epithelium in the presence or absence of CCR7. Primary and secondary sphere formation from normal (Figure 3d) or PyMT-expressing (Figure 3e) mammary cells was substantially reduced after CCR7 ablation and, importantly, stimulation of WT and WT+ cells with CCR7 ligands CCL19 and CCL21 significantly potentiated mammosphere growth (Figure 3d-e).

This CCR7 stimulatory function was seen exclusively on mammosphere growth, as stimulation with CCL19 and CCL21 had no detectable effect on the proliferation of bulk mammary tumor cells in adherent cultures, a condition that supports a more differentiated phenotype (Supplementary Figure 5c). The addition of CCR7 ligands to sphere cultures derived from CCR7 KO+ mammary cells also had no effect on MFE (Supplementary Figure 5d), demonstrating a CCR7 receptor-mediated mechanism. The specificity of CCR7 was further shown by testing a panel of ligands for other tumor-associated chemokine receptors CCR6 (16), CXCR3 (28) and CXCR5 (29). No effects were observed on MFE (Supplementary Figure 5e).

In order to extend these findings to human breast cancer we next examined the activity of CCR7 in human primary tumor cells from resected breast cancer tissue. The addition of CCL19 and CCL21 resulted in an increase in primary and secondary MFE of human breast cancer cells by 2- to 3-fold (Figure 3f), consistent with results obtained in the mouse model.

To specifically link the deletion of CCR7 to depleted tumor-initiating cells, a limiting dilution transplantation approach was used (24) to estimate tumor-initiating cell frequency. Secondary mammosphere-derived cells from WT+ and CCR7 KO+ mice with early neoplasia were used in this assay to address the potential of cells in mammosphere cultures to exhibit stem cell traits of self-renewal and tumor initiation *in vivo*, in the context of CCR7-dependency. Cells were injected into contralateral inguinal fat pads of non-PyMT WT recipients. Analysis of grafted fat pads after 6 weeks showed that WT+ sphere cells produced much more robust growth at all dilutions (Figure 4a and Supplementary Figure 6). Most importantly, the frequency of stem-like cells capable of tumor initiation within WT+ sphere culture (1/189) was over 3-fold higher than in CCR7 KO+ (1/913) (Figure 4b), providing strong evidence for the critical role of CCR7 in the regulation and maintenance of stem-like cells and tumor-initiating cells in the mammary gland.

CCR7 is required for the propagation of mammary tumors

In order to obtain *in vivo* evidence for the role of CCR7 in tumor propagation, we took advantage of the PyMT mouse model which allows tumor formation upon transplantation (20). Expression of the PyMT oncogene results in multifocal tumors and hence can generate diverse CSC pools due to various underlying mutations in different foci within the same gland at the late stages of tumourigenesis. Therefore we reasoned that if taken at the early stage of pre-neoplastic tumor development, the population of CSCs should be more homogeneous. Consequently, small $1mm^3$ fragments of pre-neoplastic mammary tissue from 8 week old PyMT transgenic WT+ and CCR7 KO+ mice were simultaneously transplanted into contralateral inguinal mammary fat pads of non-PyMT WT recipients. Representative histological sections from both WT+ and CCR7 KO+ 8 week old mice, corresponding to donor tissue, are shown in Figure 5a, confirming that the glands used for transplantation were at the equivalent stage of tumourigenesis.

Analysis of tumourigenic outgrowth from transplanted tissue showed that the deletion of CCR7 almost completely blocked secondary tumor development. Only 1 out of 6 transplants from the CCR7 KO+ donors was able to give rise to a neoplastic lesion whereas 5 out of 6 fragments from the WT+ donors produced secondary outgrowths in WT recipients (Figure 5b-c), demonstrating a key role of CCR7 in tumor propagation.

Pharmacological antagonism of CCR7 *in vivo* depletes the stem-like cell population and inhibits mammary tumourigenesis

A CCR7 antagonist, $CCL19_{(8\text{-}83)}$ (30), was employed to explore the potential of targeting CCR7 for CSC-directed therapeutic intervention. Initially, the ability of $CCL19_{(8\text{-}83)}$ to block the stimulatory activity of CCR7 ligands on mammosphere-forming capacity was tested *ex vivo* and found to specifically abrogate the effect of CCL21 (Figure 6a) and CCL19 (data not shown) on mammosphere growth providing a rationale for *in vivo* studies.

The effect of CCR7 blockade by $CCL19_{(8\text{-}83)}$ on tumor initiation was then examined in the context of the PyMT transgenic mouse model. $CCL19_{(8\text{-}83)}$ was injected for 8 consecutive weeks into inguinal mammary glands of animals from the age of 4 weeks old. Glands were then excised and examined for the extent of tumourigenesis and stem-like cell content and function. Macroscopic analysis demonstrated that $CCL19_{(8\text{-}83)}$-injected glands had smaller lesions than their control counterparts (representative image Figure 6b). The total weight of fat pads was not statistically different; however, the cellularity (total cell count and cells per mg of tissue) was significantly reduced by the antagonist (Figure 6c, Supplementary Figure 7a-b).

Treatment with $CCL19_{(8\text{-}83)}$ also resulted in a significant decrease in the proportion of stem-like cells ($Lin^-CD24^+CD29^{hi}$ Figure 6d left panel, and $Lin^-CD49f^+DLL1^+DNER^+$ Supplementary Figure 7c) and the function of stem and early progenitor cells (Figure 6d right

panel), without affecting the level of CCR7 receptor expression (Supplementary Figure 7d). Both FVB and C57B/l6 (not shown) PyMT transgenic mice were tested, with similar results.

To determine if treatment with $CCL19_{(8\text{-}83)}$ has an inhibitory effect on established and/or advanced later stage tumors, $1mm^3$ size fragments of MMTV-PyMT WT+ tumors from 16 week old mice, corresponding to the invasive ductal carcinoma stage of human breast cancer (Supplementary Figure 1a), were transplanted into inguinal glands of WT recipients followed by 8 weekly injections of $CCL19_{(8\text{-}83)}$ or vehicle control (Figure 6e left panel). Whilst no significant differences were seen between $CCL19_{(8\text{-}83)}$- or vehicle-treated tumors in size or cellularity (Supplementary Figure 7e) as was observed in primary tumors, the proportions of stem-like cells determined by both conventional ($Lin^-CD24^+CD29^{hi}$ Figure 6e center panel) or novel ($Lin^-CD49f^+DLL1^+DNER^+$ Supplementary Figure 7f) marker sets, as well as mammosphere growth (Figure 6e right panel), were significantly reduced in antagonist-treated glands, demonstrating that the CCR7 axis can be blocked *in vivo* to target stem-like cells in mammary tumors.

DISCUSSION

The contribution of CSCs to tumor initiation is a major issue in tumor biology yet one of the least understood processes (3). We show here that ablating CCR7 using a bigenic MMTV-PyMT *Ccr7*$^{-/-}$ model significantly depleted the breast cancer stem cell-enriched pool. Using the surface marker profiles $CD24^{+}CD29^{hi}$ (4) and $CD49f^{+}DLL1^{+}DNER^{+}$ (24) we showed that the underlying mechanism involves a decrease in the ability of stem-like cells and early progenitor cells to self-renew and initiate neoplasia. Significantly, exogenously targeting CCR7 with a peptide antagonist led to a decrease in tumourigenesis.

CCR7 has been extensively studied for its role in adaptive immunity and secondary lymphoid organogenesis, and CCR7-null mice display disrupted architecture of the thymus and lymph node, as well as a reduced ability to mount a primary immune response (31). The role of CCR7 in mediating anti-tumor immunity is also slowly emerging (32). In this context, the fact that abrogation of CCR7 severely affected mammary tumourigenesis provides definitive evidence of CCR7 as a pro-tumourigenic driver. Furthermore, numerous transplantation approaches used in this study underscore an immune system-independent role of this chemokine receptor in maintaining stem-like cell pools in breast cancer.

Interestingly, hyperplastic outgrowth, widely believed to be a precursor of mammary tumors (20), was found in 100% of WT and CCR7 KO PyMT-carrying glands examined. However, the majority of CCR7 KO+ glands were unable to sustain this initial proliferative burst of tumor cells and progress to the next stage in tumor development. Therefore, the delay in mammary tumourigenesis appears to be due to CCR7 maintaining specialized hierarchical sub-populations of cancer stem and progenitor-like cells that are thought to be crucial for tumor initiation and advanced tumourigenesis (2).

The fact that both CCL19 and CCL21 stimulated mammosphere growth from both human and mouse tumor cells strongly suggests that CCR7 plays a global role in sustaining

properties of stemness in mammary epithelium. The specificity of CCR7 in this process was validated through testing a panel of chemokine receptor ligands, where only CCL19 and CCL21 showed an ability to significantly increase mammosphere-forming efficiency.

Stimulation of CXCR4, the chemokine receptor that is consistently found to be upregulated together with CCR7 in a number of cancers (17), did potentiate sphere formation but to a lesser extent (Supplementary Figure 5e). Recently, Clarke and colleagues demonstrated that stimulation of CXCR4 also increased MFE preferentially in malignant breast cancer cell lines compared to normal breast cell lines (26). It is interesting to speculate that as CCR7 is less important for homeostasis than CXCR4, as has been inferred from animal models (33), CCR7 may represent a more attractive target for future CSC-targeting therapies.

As stimulation of CCR7 had no effect on proliferation of the bulk population of cells when seeded into adherent culture, compared to a highly significant effect in non-adherent culture, it is likely that CCR7 predominantly mediates specific cellular properties of stemness. Moreover, we have previously reported that CCR7 activation on breast cancer cells inhibits anoikis (13), a characteristic of breast and other CSCs (25, 34). Therefore, it is plausible that CCR7 supports CSC survival without attachment to the extracellular matrix, a hypothesis which may form the basis for future studies.

CCR7 appeared to play a quantitative rather than a qualitative role in normal mammary stem cells compared to cancer stem cells. Upon deletion of CCR7 we saw a mild effect on the normal mammary gland. In contrast, a major effect was seen in mammary tumourigenesis. Interestingly, whilst the morphological effect on normal mammary gland development was not extensive, CCR7 deletion discreetly affected normal mammary gland stem-like cells. Therefore, it is plausible that CCR7 has a role in regulating the properties of stemness within the mammary epithelial cell population, an effect which appears more

prominent during cancer progression. As highlighted in a recent study by Cheresh and colleagues (35), dysregulation of normal stem cells may contribute to breast cancer progression and stemness, and CCR7 may emerge as a novel mediator of this transition.

Translation of our findings from the mouse model to human disease is of particular significance considering that there is currently no clear consensus on the markers that define functional mammary stem cells in both mice and humans. Thus we show here that CCR7 not only plays a role in mouse mammary tissue, but is also expressed, is functional, and is highly responsive in the stem-like populations within human breast cancer tissue. Intriguingly, circulating tumor cells, an indicator of metastatic spread and poor outcome in breast and other cancers, have been recently equated to CSCs (36). In the last decade numerous studies also suggested a role for CCR7 in malignant dissemination of mammary tumors to distant sites (13, 15, 17). Taken together, these results suggest a novel causative link between CCR7 activity on stem-like populations and metastatic breast cancer.

In order to seek proof-of-principle on the utility of pharmacologically targeting CCR7 we tested the receptor antagonist $CCL19_{(8\text{-}83)}$ (30). We found that pharmacological inhibition of CCR7 through direct mammary fat pad injection of $CCL19_{(8\text{-}83)}$ afforded a significant reduction in early stage primary mammary tumourigenesis. Since the relative contribution of the malignant lesions to the weight of the whole mammary fat pad was very small at this early stage the reduction in total weight between antagonist and vehicle treated glands was not statistically significant. However the cellularity, a characteristic that directly reflects the extent of epithelial malignant outgrowth and is used in clinical pathology to evaluate the response to chemotherapy in breast cancer, was strongly impacted by treatment with the CCR7 antagonist.

More importantly, directly targeting CCR7 using the antagonist significantly depleted the stem-like cell pools in both early and late stage mammary neoplasia as was shown using

the transplantation approach. These findings strongly suggest that the CCR7 receptor axis is a potential point of intervention in stem cell-targeting therapies and provide a rationale for the use of antagonists of this pathway as adjuvants to conventional cytotoxic drugs unable to eliminate quiescent cancer stem cells (2).

In conclusion, the characterization of CCR7 in primary breast tumourigenesis *in vitro* and *in vivo*, and in mouse and human tissue, strongly suggests a role for this molecule in breast cancer development and progression. These insights raise the possibility of pharmacologically targeting CCR7 for the development of new therapies in breast cancer.

MATERIALS and METHODS

Mice

Mice were maintained in pathogen-free conditions in the University of Adelaide's Laboratory Animal Services facility. *Ccr7*$^{-/-}$ mice were purchased from Jackson Laboratory. FVB MMTV-PyMT (+) mice were backcrossed for 14 generations to C57Bl/6 background, and C57Bl/6 background was confirmed by microsatellite analysis. PyMT-carrying males were then crossed with *Ccr7*$^{-/-}$ females, and the offspring were interbred to produce MMTV-PyMT *Ccr7*^{WT} and MMTV-PyMT *Ccr7*$^{-/-}$ mice. The University of Adelaide institutional animal ethics committee approved all experimentation. For the assessment of CCR7 expression and CCL19$_{(8-83)}$ function both C57Bl/6 and FVB backgrounds were tested to eliminate any strain bias. For experiments involving knock-out mice, only C57Bl/6 mice were tested. Nomenclature used for genotypes is as follows: *Ccr7*^{WT} = WT, *Ccr7*$^{-/-}$ = CCR7 KO, MMTV-PyMT *Ccr7*^{WT} = WT+, MMTV-PyMT *Ccr7*$^{-/-}$ = CCR7 KO+.

Human Mammary Tissue

Ethical approval was granted by the Royal Adelaide Hospital Ethics Committee and all patients gave written, informed consent prior to surgery. Pathology reports for tumors used are available upon request. Normal breast tissue samples were obtained from the Queen Elizabeth Hospital, Adelaide.

Whole Mount Staining

Mammary glands were fixed in Carnoy's and were stained overnight in Carmine Alum before dehydration and mounting. Image "stitching" and analysis was performed using Image J.

Histology

Lungs of MMTV-PyMT WT+ or CCR7 KO+ mice were perfused and dissected, then embedded and frozen in OCT and serially sectioned at 9μm. Formalin-fixed paraffin-

embedded (FFPE) mammary glands/tumors were sectioned at 5μm. All slides were stained using haemotoxylin and eosin (H&E), dehydrated and mounted. Slides were scanned using the NanoZoomer Digital Pathology (NDP) System (Hamamatsu Photonics) and lung sections were manually quantitated using the NDP Virtual Slide Viewer software for number of metastases and area at the largest point.

Immunofluorescent Microscopy

Antigen retrieval of FFPE mouse mammary sections was performed by boiling slides in 0.1 M sodium citrate buffer (pH 6.0). Slides were stained with rabbit anti-CCR7 (Epitomics) overnight at 4°C, and primary antibody was detected with Alexa Fluor 488-conjugated goat anti-rabbit (Invitrogen) for 30 minutes. Slides were counterstained with DAPI, mounted, and analyzed using the Leica TCS SP5 Confocal Microscope System.

Processing Mouse Mammary Tissue to Single Cell Suspension

Mouse mammary glands/tumors were dissected, with removal of the lymph node if possible. Tissue was manually dissociated and then digested in 10% collagenase/hyaluronidase (Stem Cell Technologies) for 3-4 hours with gentle tilting. Single cells were extracted as previously described (37) and filtered through a 70μm nylon mesh. In order to remove contaminating infiltrating cells of hematopoietic origin, Biotin Binder Dynabeads (Invitrogen) in combination with a biotinylated anti-mouse lineage antibody panel (BioLegend), were used as suggested by the manufacturer.

Processing Human Mammary Tissue to Single Cell Suspension

Surgical specimens were minced and digested in 10% collagenase/hyaluronidase (Stem Cell Technologies) in DMEM supplemented with 20mM HEPES, penicillin-streptomycin, and 0.25μg/ml fungazone. Organoids were then extensively washed with DMEM and red blood cells were lysed by isotonic lysis buffer (150mM NH_4Cl in 17mM Tris-HCl, pH 7.2). Single cell suspensions were obtained by digesting organoids with 0.25%

trypsin for 10 minutes at room temperature, with subsequent filtration through a 70μm nylon mesh.

Flow Cytometry

Cells were fixed in 4% paraformaldehyde and immunostained for 45 minutes on ice in PBS/0.5%BSA. Antibodies used were: Alexa Fluor 647-conjugated anti-mouse CCR7, PE-conjugated anti-mouse/anti-human CD24, FITC/PECy5-conjugated anti-human CD49f, FITC-conjugated anti-human CD44 (all from BD), FITC-conjugated anti-mouse CD29, PE-conjugated anti-mouse/anti-human DLL1 (all from BioLegend), and biotinylated anti-mouse/anti-human DNER (R&D). Samples containing biotinylated antibodies were resuspended in PerCP/Cy5.5 or Alexa Fluor 488-conjugated streptavidin (1/1000 dilution) in PBS/0.5% BSA for 30 minutes on ice. Fluorescence-minus-one (FMO) samples or conjugated isotypes were used as negative controls. Flow cytometry was carried out using FACSCanto equipment (BD). Data analysis was performed using FlowJo software (Tree Star Inc.).

Mammosphere Assay

Cells were seeded in mammosphere medium (1:1 mixture of DMEM and Ham's F12 medium (Gibco) supplemented with 1xB27 (Invitrogen), 20ng/ml EGF, 20ng/ml bFGF, 4μg/ml heparin (Sigma-Aldrich), penicillin-streptomycin, and 0.25μg/ml fungazone) at $4x10^4$cells/ml to an ultra-low attachment tray (Corning). Where indicated, CCL21, CCL19 and $CCL19_{(8-83)}$ were added at concentrations of 10ng/ml, 200ng/ml and 100ng/ml respectively. Media was replenished every second day. After 7-10 days, mammospheres were counted and passaged.

Limiting Dilution Assay

Mammosphere colonies derived from 8 week old pre-neoplastic MMTV-PyMT WT+ and CCR7 KO+ mice were dissociated using trypsin and triturated through a 19G needle.

Following filtration, cells were injected in 20% Matrigel (BD):80% DMEM into the fourth inguinal mammary glands of anaesthetized WT recipient mice (8 weeks old) at limiting dilutions as previously described (24). Mice were sacrificed after 6 weeks and glands whole-mounted. TIC-frequency and statistical calculations were performed using L-Calc software (Stem Cell Technologies).

Tissue Transplants

Mammary gland fragments of $1mm^3$ size from donor MMTV-PyMT mice were transplanted into contralateral sides of anaesthetized congenic non-PyMT WT recipient mice (8 weeks old) within the fourth inguinal mammary glands. Mice were monitored for adverse reactions to surgery and subsequent tumor growth.

***In vivo* Treatment with CCR7 Antagonist**

Mice were injected under anesthetic into an inguinal mammary fat pad, with 1μg $CCL19_{(8\text{-}83)}$ truncated ligand in 50μl saline vehicle, as indicated. As a control, mice were injected in the contralateral inguinal mammary fat pad with vehicle alone as previously reported (38, 39).

Statistical Analysis

Unless otherwise indicated, analyses were carried out using GraphPad Prism and data is shown as mean ± SEM. Significant statistical difference was estimated using student's t-tests, or chi-square tests for distribution analysis. Tumor-free survival curves were graphed using the Kaplan-Meier method and distributions were compared by the log-rank statistic (Mantel-Cox test). All measurements were done in triplicate. P-values were used to denote statistical significance. Levels of significance were $*p \leq 0.05$, $**p \leq 0.01$, and $***p \leq 0.001$.

CONFLICTS OF INTEREST STATEMENT: The authors declare no conflict of interest.

ACKNOWLEDGEMENTS

We are grateful to Dr. Timothy Proudman and Dr. Pallave Dasari from the Queen Elizabeth Hospital for supply of normal human breast tissue and Dr. Deepak Dhatrak of the Department of Anatomical Pathology at SA Pathology for procurement of human breast cancer samples. We would also like to sincerely thank Professor Angel Lopez for critical reading of the manuscript, and Dr. Michael Samuel and Ms. Natasha Pyne for assistance with immunohistochemistry. This work was supported by an NHMRC project grant. WVI is a National Breast Cancer Foundation/The QEH Research Foundation Fellow.

SUPPLEMENTARY INFORMATION

Supplementary Information accompanies the paper on the *Oncogene* website (http://www.nature.com/onc).

REFERENCES

1. Maxmen A. The hard facts. Nature. 2012;485(7400):S50-1.

2. Visvader JE, Lindeman GJ. Cancer stem cells: current status and evolving complexities. Cell stem cell. 2012;10(6):717-28.

3. Medema JP. Cancer stem cells: the challenges ahead. Nat Cell Biol. 2013;15(4):338-44.

4. Visvader JE. Keeping abreast of the mammary epithelial hierarchy and breast tumorigenesis. Genes Dev. 2009;23(22):2563-77. Epub 2009/11/26.

5. Bouras T, Pal B, Vaillant F, Harburg G, Asselin-Labat ML, Oakes SR, et al. Notch signaling regulates mammary stem cell function and luminal cell-fate commitment. Cell stem cell. 2008;3(4):429-41. Epub 2008/10/23.

6. Liu S, Dontu G, Mantle ID, Patel S, Ahn NS, Jackson KW, et al. Hedgehog signaling and Bmi-1 regulate self-renewal of normal and malignant human mammary stem cells. Cancer Res. 2006;66(12):6063-71. Epub 2006/06/17.

7. van Amerongen R, Bowman AN, Nusse R. Developmental stage and time dictate the fate of Wnt/beta-catenin-responsive stem cells in the mammary gland. Cell Stem Cell. 2012;11(3):387-400.

8. Iwanaga R, Wang CA, Micalizzi DS, Harrell JC, Jedlicka P, Sartorius CA, et al. Expression of Six1 in luminal breast cancers predicts poor prognosis and promotes increases in tumor initiating cells by activation of extracellular signal-regulated kinase and transforming growth factor-beta signaling pathways. Breast cancer research : BCR. 2012;14(4):R100.

9. Chin AR, Wang SE. Cytokines driving breast cancer stemness. Molecular and cellular endocrinology. 2014;382(1):598-602.

10. Balkwill FR. The chemokine system and cancer. J Pathol. 2012;226(2):148-57.

11. Muller A, Homey B, Soto H, Ge N, Catron D, Buchanan ME, et al. Involvement of chemokine receptors in breast cancer metastasis. Nature. 2001;410(6824):50-6. Epub 2001/03/10.

12. Li J, Sun R, Tao K, Wang G. The CCL21/CCR7 pathway plays a key role in human colon cancer metastasis through regulation of matrix metalloproteinase-9. Dig Liver Dis. 2011;43(1):40-7. Epub 2010/07/09.

13. Kochetkova M, Kumar S, McColl SR. Chemokine receptors CXCR4 and CCR7 promote metastasis by preventing anoikis in cancer cells. Cell death and differentiation. 2009;16(5):664-73. Epub 2009/01/13.

14. Cunningham HD, Shannon LA, Calloway PA, Fassold BC, Dunwiddie I, Vielhauer G, et al. Expression of the C-C chemokine receptor 7 mediates metastasis of breast cancer to the lymph nodes in mice. Transl Oncol. 2010;3(6):354-61. Epub 2010/12/15.

15. Andre F, Cabioglu N, Assi H, Sabourin JC, Delaloge S, Sahin A, et al. Expression of chemokine receptors predicts the site of metastatic relapse in patients with axillary node positive primary breast cancer. Annals of oncology : official journal of the European Society for Medical Oncology / ESMO. 2006;17(6):945-51. Epub 2006/04/22.

16. Cassier PA, Treilleux I, Bachelot T, Ray-Coquard I, Bendriss-Vermare N, Menetrier-Caux C, et al. Prognostic value of the expression of C-Chemokine Receptor 6 and 7 and their ligands in non-metastatic breast cancer. BMC Cancer. 2011;11:213. Epub 2011/06/01.

17. Cabioglu N, Yazici MS, Arun B, Broglio KR, Hortobagyi GN, Price JE, et al. CCR7 and CXCR4 as novel biomarkers predicting axillary lymph node metastasis in T1 breast cancer. Clinical cancer research : an official journal of the American Association for Cancer Research. 2005;11(16):5686-93. Epub 2005/08/24.

18. Lin EY, Jones JG, Li P, Zhu L, Whitney KD, Muller WJ, et al. Progression to malignancy in the polyoma middle T oncoprotein mouse breast cancer model provides a

reliable model for human diseases. The American journal of pathology. 2003;163(5):2113-26. Epub 2003/10/28.

19. Guy CT, Cardiff RD, Muller WJ. Induction of mammary tumors by expression of polyomavirus middle T oncogene: a transgenic mouse model for metastatic disease. Mol Cell Biol. 1992;12(3):954-61. Epub 1992/03/01.

20. Maglione JE, Moghanaki D, Young LJ, Manner CK, Ellies LG, Joseph SO, et al. Transgenic Polyoma middle-T mice model premalignant mammary disease. Cancer research. 2001;61(22):8298-305.

21. Schwab LP, Peacock DL, Majumdar D, Ingels JF, Jensen LC, Smith KD, et al. Hypoxia-inducible factor 1alpha promotes primary tumor growth and tumor-initiating cell activity in breast cancer. Breast cancer research : BCR. 2012;14(1):R6.

22. Ma J, Lanza DG, Guest I, Uk-Lim C, Glinskii A, Glinsky G, et al. Characterization of mammary cancer stem cells in the MMTV-PyMT mouse model. Tumour biology : the journal of the International Society for Oncodevelopmental Biology and Medicine. 2012;33(6):1983-96.

23. Al-Hajj M, Wicha MS, Benito-Hernandez A, Morrison SJ, Clarke MF. Prospective identification of tumorigenic breast cancer cells. Proc Natl Acad Sci U S A. 2003;100(7):3983-8. Epub 2003/03/12.

24. Pece S, Tosoni D, Confalonieri S, Mazzarol G, Vecchi M, Ronzoni S, et al. Biological and molecular heterogeneity of breast cancers correlates with their cancer stem cell content. Cell. 2010;140(1):62-73. Epub 2010/01/16.

25. Dontu G, Abdallah WM, Foley JM, Jackson KW, Clarke MF, Kawamura MJ, et al. In vitro propagation and transcriptional profiling of human mammary stem/progenitor cells. Genes Dev. 2003;17(10):1253-70. Epub 2003/05/21.

26. Ablett MP, O'Brien CS, Sims AH, Farnie G, Clarke RB. A differential role for CXCR4 in the regulation of normal versus malignant breast stem cell activity. Oncotarget. 2014;5(3):599-612.

27. Pastrana E, Silva-Vargas V, Doetsch F. Eyes wide open: a critical review of sphere-formation as an assay for stem cells. Cell stem cell. 2011;8(5):486-98.

28. Ma X, Norsworthy K, Kundu N, Rodgers WH, Gimotty PA, Goloubeva O, et al. CXCR3 expression is associated with poor survival in breast cancer and promotes metastasis in a murine model. Mol Cancer Ther. 2009;8(3):490-8.

29. Biswas S, Sengupta S, Roy Chowdhury S, Jana S, Mandal G, Mandal PK, et al. CXCL13-CXCR5 co-expression regulates epithelial to mesenchymal transition of breast cancer cells during lymph node metastasis. Breast Cancer Res Treat. 2014;143(2):265-76.

30. Pilkington KR, Clark-Lewis I, McColl SR. Inhibition of generation of cytotoxic T lymphocyte activity by a CCL19/macrophage inflammatory protein (MIP)-3beta antagonist. J Biol Chem. 2004;279(39):40276-82.

31. Forster R, Schubel A, Breitfeld D, Kremmer E, Renner-Muller I, Wolf E, et al. CCR7 coordinates the primary immune response by establishing functional microenvironments in secondary lymphoid organs. Cell. 1999;99(1):23-33. Epub 1999/10/16.

32. Sharma S, Stolina M, Luo J, Strieter RM, Burdick M, Zhu LX, et al. Secondary lymphoid tissue chemokine mediates T cell-dependent antitumor responses in vivo. Journal of immunology. 2000;164(9):4558-63.

33. Zou YR, Kottmann AH, Kuroda M, Taniuchi I, Littman DR. Function of the chemokine receptor CXCR4 in haematopoiesis and in cerebellar development. Nature. 1998;393(6685):595-9.

34. Luo M, Guan JL. Focal adhesion kinase: a prominent determinant in breast cancer initiation, progression and metastasis. Cancer letters. 2010;289(2):127-39.

35. Desgrosellier JS, Lesperance J, Seguin L, Gozo M, Kato S, Franovic A, et al. Integrin alphavbeta3 drives slug activation and stemness in the pregnant and neoplastic mammary gland. Developmental cell. 2014;30(3):295-308.

36. Giordano A, Gao H, Cohen EN, Anfossi S, Khoury J, Hess K, et al. Clinical relevance of cancer stem cells in bone marrow of early breast cancer patients. Annals of oncology : official journal of the European Society for Medical Oncology / ESMO. 2013;24(10):2515-21.

37. Smalley MJ, Kendrick H, Sheridan JM, Regan JL, Prater MD, Lindeman GJ, et al. Isolation of Mouse Mammary Epithelial Subpopulations: A Comparison of Leading Methods. J Mammary Gland Biol Neoplasia. 2012. Epub 2012/05/31.

38. Lavergne E, Combadiere C, Iga M, Boissonnas A, Bonduelle O, Maho M, et al. Intratumoral CC chemokine ligand 5 overexpression delays tumor growth and increases tumor cell infiltration. J Immunol. 2004;173(6):3755-62.

39. Weninger W, Carlsen HS, Goodarzi M, Moazed F, Crowley MA, Baekkevold ES, et al. Naive T cell recruitment to nonlymphoid tissues: a role for endothelium-expressed CC chemokine ligand 21 in autoimmune disease and lymphoid neogenesis. J Immunol. 2003;170(9):4638-48.

FIGURE LEGENDS

Figure 1: CCR7 deletion arrests mammary tumourigenesis in the PyMT transgenic breast cancer mouse model

(**a-c**) CCR7 ablation delays tumor onset and reduces tumor burden in the MMTV-PyMT-driven mouse model of breast cancer. (**a**) Representative images of MMTV-PyMT *Ccr7*^{WT} (WT+) and MMTV-PyMT *Ccr7*$^{-/-}$ (CCR7 KO+) mice at 22 weeks old, showing grossly visible tumors (demarcated by red arrows and dotted lines). (**b**) Kaplan-Meier analysis of tumor-free survival for WT+ (n=18) and CCR7 KO+ (n=17) mice. (**c**) Number of tumors in WT+ and CCR7 KO+ mice at the time of sacrifice. (**d-f**) CCR7 KO+ mice developed less lung metastases than their WT+ counterparts. (**d**) Total cumulative area of lung metastatic lesions in WT+ (n=8) and CCR7 KO+ (n=8) mice. (**e**) Distribution data of lung metastases in WT+ and CCR7 KO+ mice. (**f**) Representative images of H&E stained lung sections from WT+ (left) and CCR7 KO+ (right) mice with metastatic lesions (black arrowheads). Red arrowhead indicates inset magnified image.

Figure 2: The effect of CCR7 on normal mammary development

(**a-b**) Development of the mammary ductal tree was evaluated in *Ccr7*^{WT} (WT) and *Ccr7*$^{-/-}$ (CCR7 KO) C57Bl/6 mice at 6 weeks of age. (**a**) Representative whole mount images of mammary glands, with apparent reduction in the size of ductal trees in CCR7 KO (right, n=6) compared to WT (left, n=7). LN= lymph node. (**b**) Quantitation of the length of the main epithelial duct (left), total number of mammary epithelial terminal structures (center), and branch points within mammary epithelium determined by quantifying branch points per mm along three individual ducts (right). (**c**) CCR7 expression (magenta) in normal mouse mammary terminal end buds of pubertal mice. Nuclei are counterstained with DAPI (gray). (**d**) Representative whole mount images of mammary glands taken from adult WT (left, n=6)

and CCR7 KO (right, n=6) mice at 12 weeks of age with no apparent differences in the size and architecture of the mammary tree.

Figure 3: CCR7 activity amplifies stem-like cells in both mouse and human mammary glands

(**a-c**) Normal mammary glands and mammary tumors were analyzed by flow cytometry for stem-like cell content. (**a**) Proportion of cells positive for CCR7 in Lin^- stem cell-enriched populations in normal mouse mammary epithelium (left) and PyMT-expressing glands (right), as denoted by surface marker expression $CD24^+CD29^{hi}$. Shaded histograms= fluorescence-minus-one negative gates. (**b**) Proportion of cells positive for CCR7 in putative stem-like cell populations in normal human mammary epithelium (left) and breast cancer (right), as denoted by surface marker expression $CD44^+CD24^-$. (**c**) CCR7 deletion decreases the proportion of mouse Lin^- stem cell-enriched populations in normal (left) and PyMT-expressing (right) mammary glands as indicated. (**d-f**) The effect of CCR7 deletion/activation on primary and secondary mammosphere formation was assessed. Shown are mammosphere-forming efficiencies of cells derived from normal mouse mammary glands (**d**), PyMT-expressing mouse mammary glands (**e**), and human patient-derived breast tumors (**f**). WT mouse cells and primary human cells were stimulated with CCL21 and CCL19 as indicated. (**a-f**) Mouse data are representative of at least 3 independent experiments, n=6-10 mice per group. Human results are representative of 2 normal and 4 independent tumor samples.

Figure 4: CCR7 increases *in vivo* tumor-initiating capacity of sphere cells

(**a**) Representative images of intact and respective whole-mounted contralateral mammary glands engrafted with 2500 WT+ or CCR7 KO+ sphere-derived cells. Black arrowheads indicate areas of outgrowth from engrafted cells. LN= lymph node. (**b**) Results of limiting dilution assay indicating frequency of tumor-initiating cells (TIC) in WT+ and CCR7 KO+

sphere cultures. Fractions indicate the number of fat pads with lesion(s) per total number of recipient fat pads.

Figure 5: CCR7 is required for the propagation of mammary tumors

(**a**) Representative H&E stained sections of pre-neoplastic mice at the WT+ and CCR7 KO+ donor age of 8 weeks. Bottom: Magnified images of boxed area. (**b**) Representative whole-mount images of WT recipient glands after transplantation of pre-neoplastic mammary tissue from WT+ (top) and CCR7 KO+ (bottom) donor mice at 8 weeks of age. Black arrowheads indicate areas of outgrowth from donor tissue. Fractions indicate the number of fat pads with lesion(s) per total number of recipient fat pads. LN= lymph node. (**c**) Cumulative area of transplant outgrowth in recipient mammary glands. n=6 mice per group.

Figure 6: Pharmacological antagonism of CCR7 *in vivo* depletes the stem-like cell population and inhibits mammary tumourigenesis

(**a**) MFE of Lin^- mammary cells from WT+ mice (n=9), untreated or treated with CCL21 and/or the CCR7 antagonist $CCL19_{(8-83)}$. (**b-d**) Treatment of mice with $CCL19_{(8-83)}$ reduces tumourigenesis in MMTV-PyMT WT+ mice. (**b**) Representative image of intact mammary glands treated with vehicle or $CCL19_{(8-83)}$ as indicated. (**c**) Cellularity of contralateral vehicle- or $CCL19_{(8-83)}$- treated glands. (**d**) Proportions of $Lin^-CD24^+CD29^{hi}$ cells (left) and MFE (right) of cells from vehicle- or $CCL19_{(8-83)}$- treated glands. (**e**) Treatment of mice with $CCL19_{(8-83)}$ reduces the stem cell-enriched population in a transplant model. Experimental strategy (left), proportion of $Lin^-CD24^+CD29^{hi}$ cells (center) and MFE (right) of cells from transplanted tumors with or without $CCL19_{(8-83)}$ treatment. (**b-e**) Data are representative of 2 independent experiments, n=4-6 mice per experiment.

Figure 1

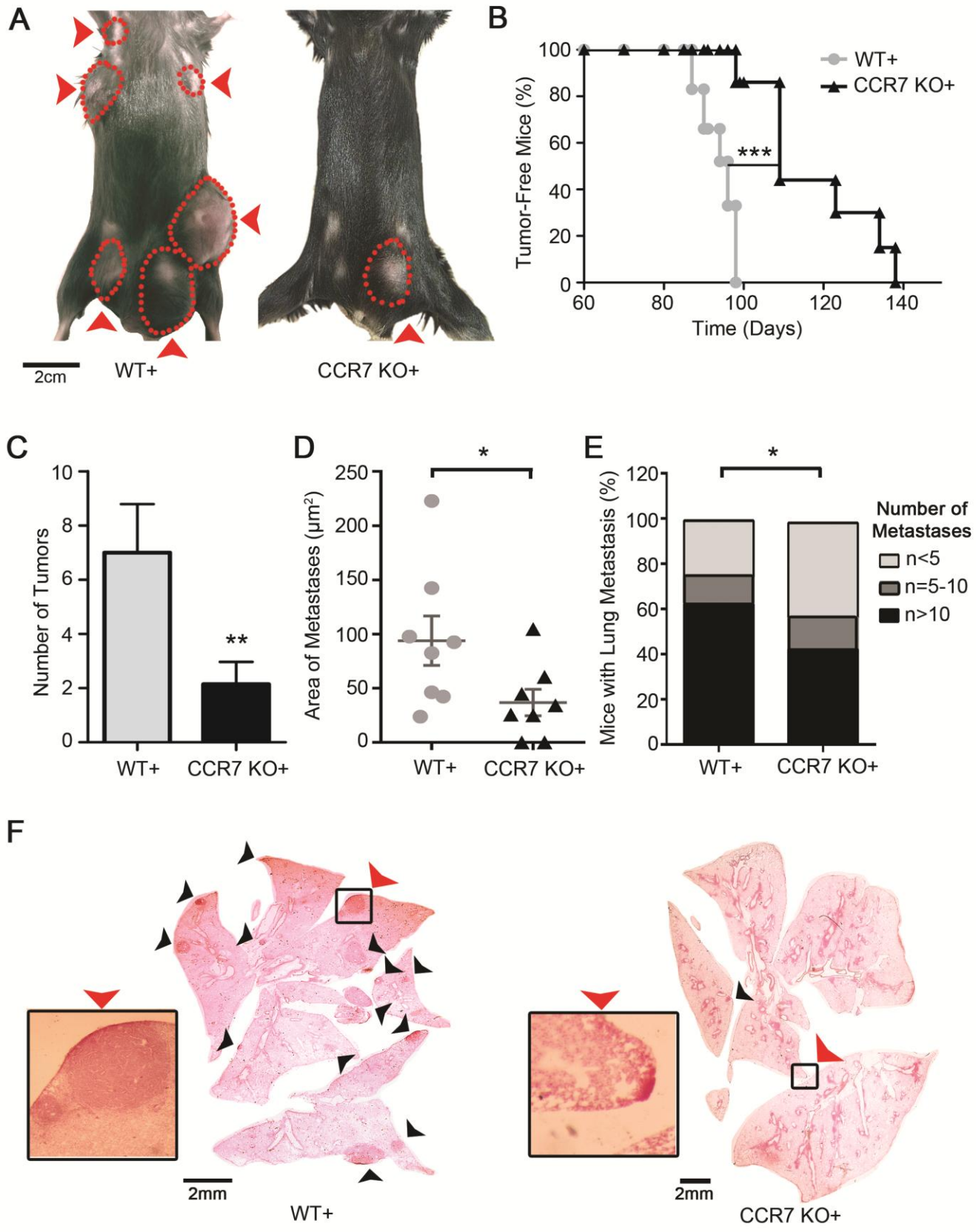
A
2cm
WT+
CCR7 KO+
B
Tumor-Free Mice (%)
Time (Days)
WT+
CCR7 KO+
***
C
Number of Tumors
**
D
Area of Metastases (μm²)
*
E
Mice with Lung Metastasis (%)
*
Number of Metastases
n<5
n=5-10
n>10
F
2mm
WT+
2mm
CCR7 KO+

Figure 2

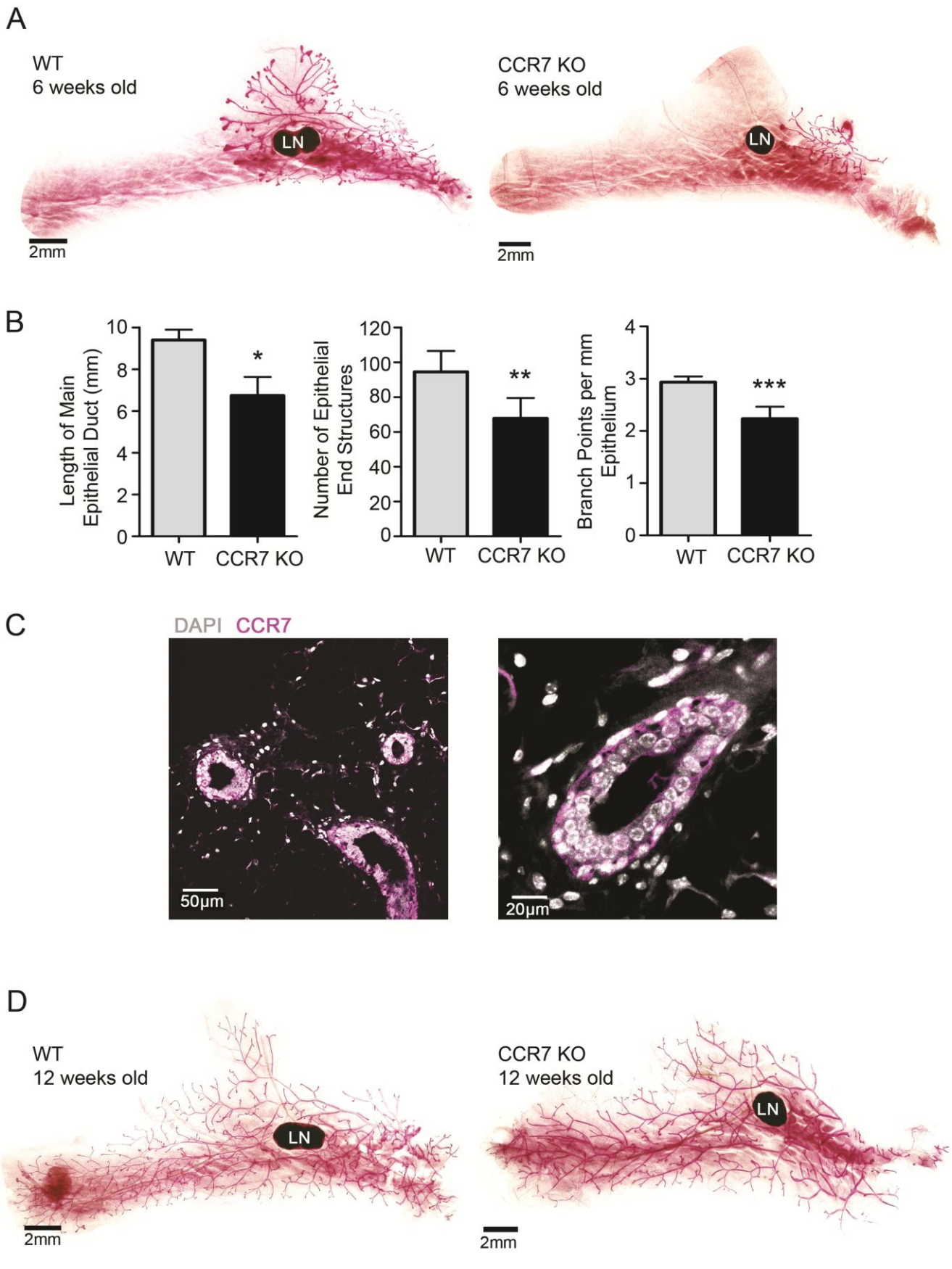
A
WT
6 weeks old
LN
2mm
CCR7 KO
6 weeks old
LN
2mm
B
Length of Main Epithelial Duct (mm)
10
8
6
4
2
0
*
WT
CCR7 KO
Number of Epithelial End Structures
120
100
80
60
40
20
0
**
WT
CCR7 KO
Branch Points per mm Epithelium
4
3
2
1
0
***
WT
CCR7 KO
C
DAPI CCR7
50µm
20µm
D
WT
12 weeks old
LN
2mm
CCR7 KO
12 weeks old
LN
2mm

Figure 3

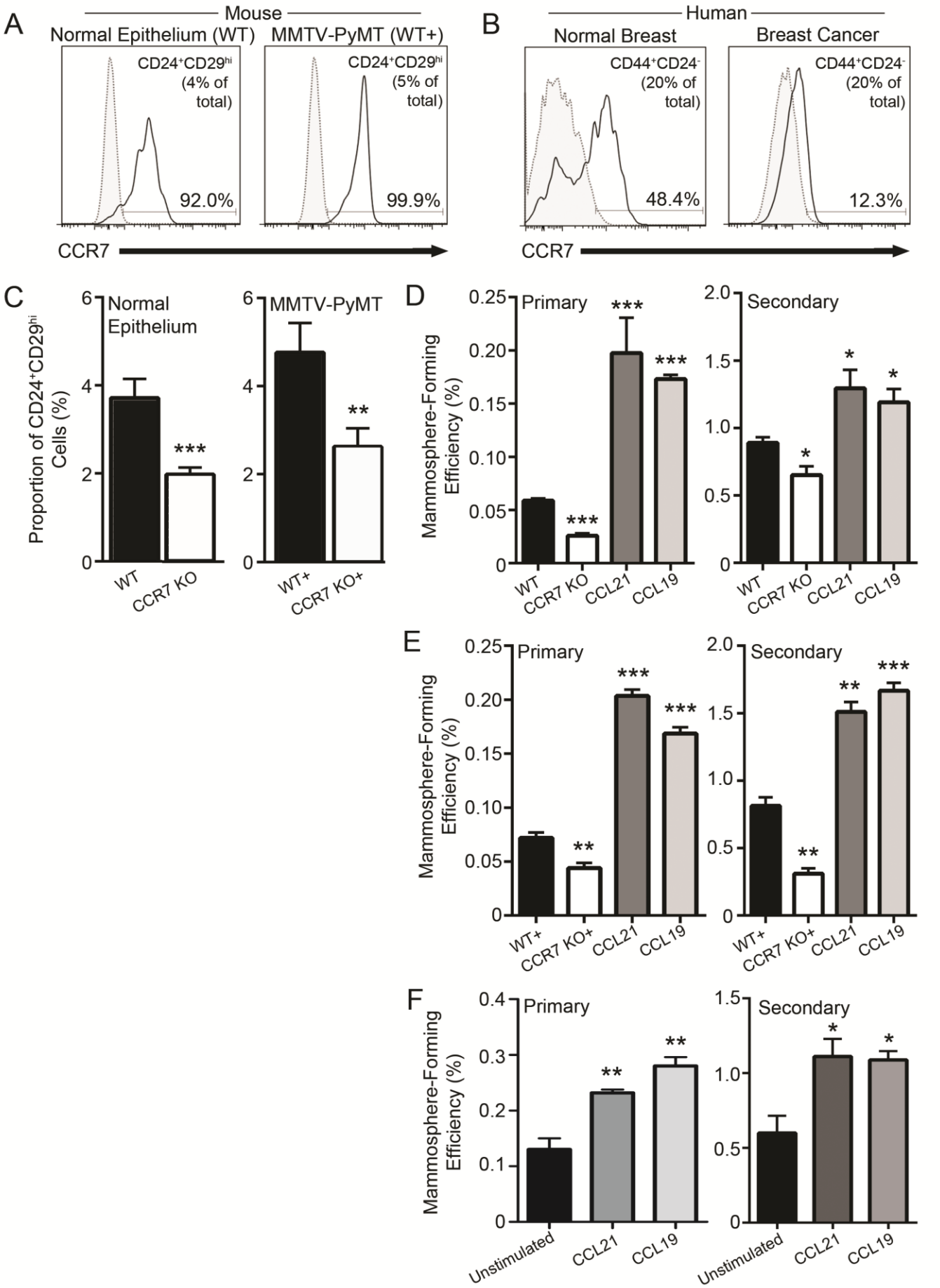
A
Mouse
Normal Epithelium (WT)
MMTV-PyMT (WT+)
CD24+CD29hi (4% of total)
92.0%
CD24+CD29hi (5% of total)
99.9%
CCR7
B
Human
Normal Breast
Breast Cancer
CD44+CD24- (20% of total)
48.4%
CD44+CD24- (20% of total)
12.3%
CCR7
C
Proportion of CD24+CD29hi Cells (%)
Normal Epithelium
MMTV-PyMT
WT
CCR7 KO
WT+
CCR7 KO+
D
Mammosphere-Forming Efficiency (%)
Primary
Secondary
WT
CCR7 KO
CCL21
CCL19
E
Mammosphere-Forming Efficiency (%)
Primary
Secondary
WT+
CCR7 KO+
CCL21
CCL19
F
Mammosphere-Forming Efficiency (%)
Primary
Secondary
Unstimulated
CCL21
CCL19

Figure 4

A

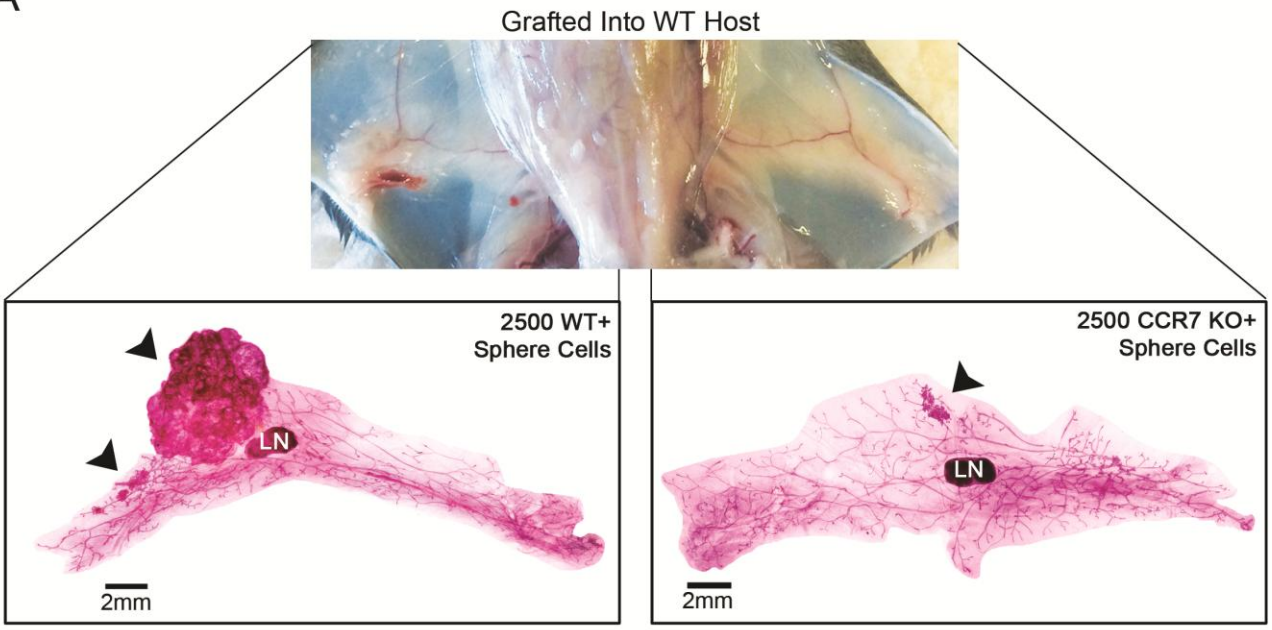

B

Number of Grafted Sphere-Derived Cells

Donor	2500	500	100	10	TIC Frequency	Range ± SE
WT+	4/4	3/4	3/5	1/4	1/189*	117-306
CCR7 KO+	3/4	3/4	1/5	0/4	1/913	563-1480

*p=0.0104

Figure 5

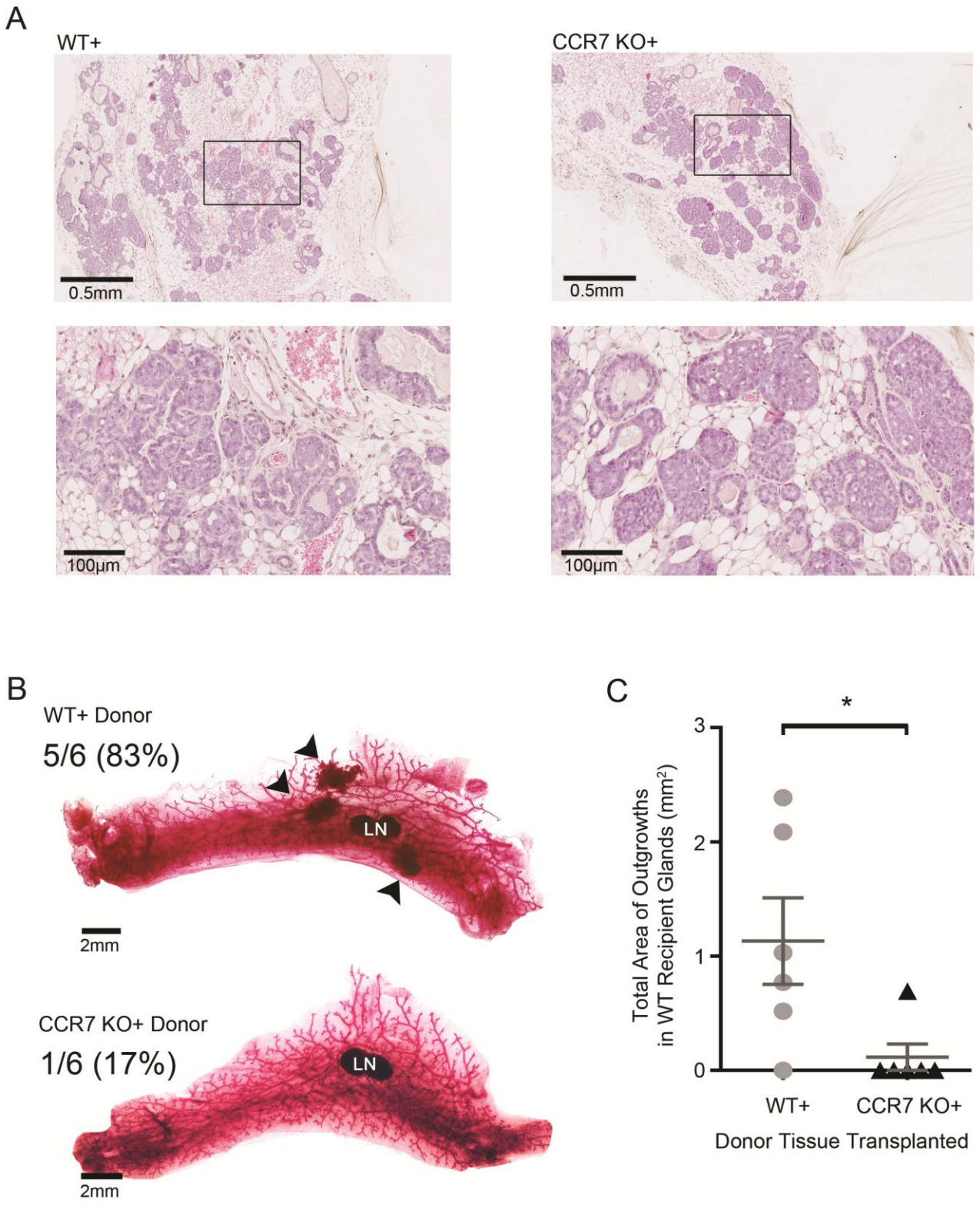
A
WT+
CCR7 KO+
0.5mm
0.5mm
100μm
100μm
B
WT+ Donor
5/6 (83%)
LN
2mm
CCR7 KO+ Donor
1/6 (17%)
LN
2mm
C
*
Total Area of Outgrowths in WT Recipient Glands (mm²)
3
2
1
0
WT+
CCR7 KO+
Donor Tissue Transplanted

Figure 6

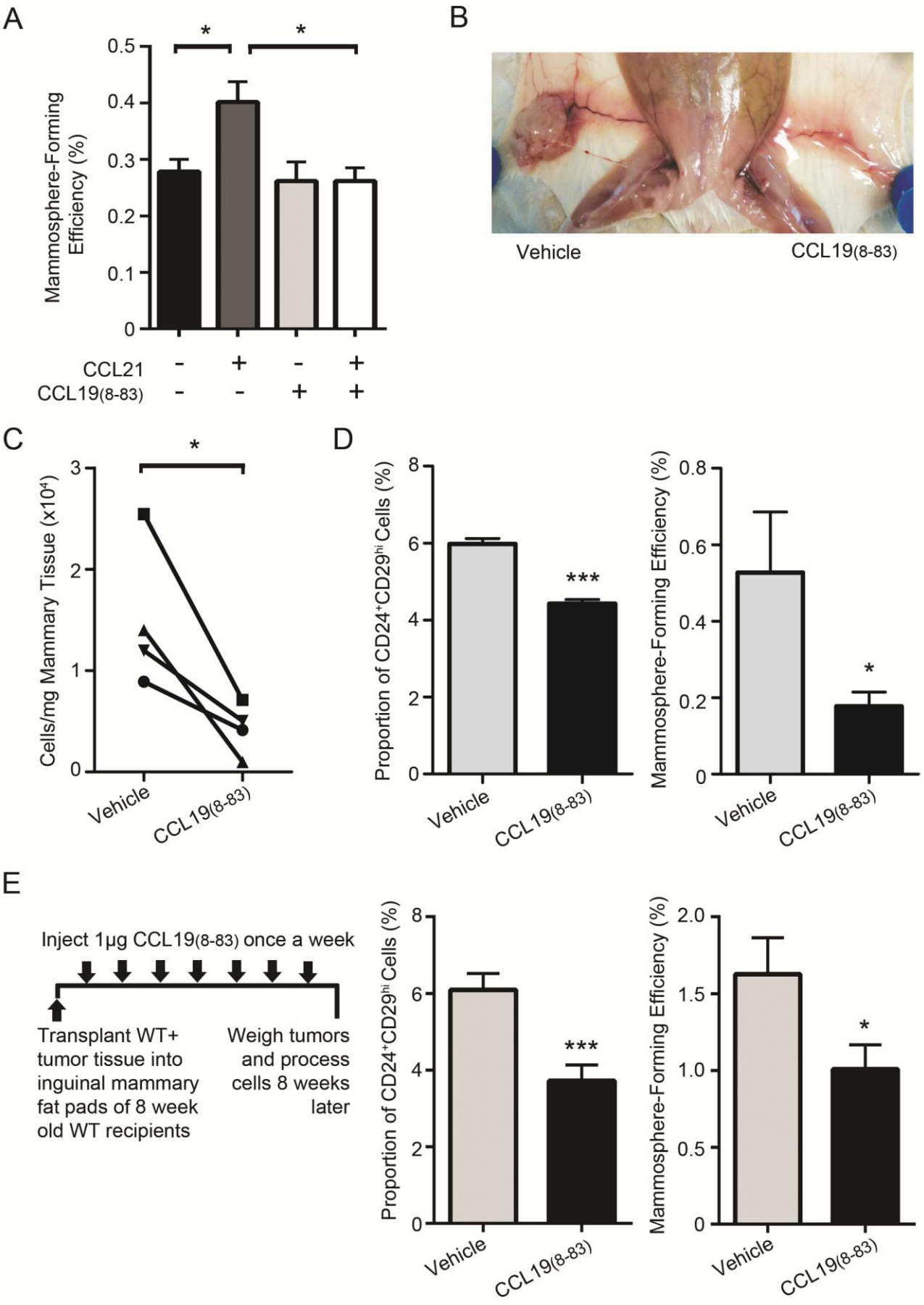
A
Mammosphere-Forming Efficiency (%)
0.5
0.4
0.3
0.2
0.1
0
*
*
CCL21 - + - +
CCL19(8-83) - - + +
B
Vehicle
CCL19(8-83)
C
Cells/mg Mammary Tissue (x10⁴)
3
2
1
0
*
Vehicle
CCL19(8-83)
D
Proportion of CD24⁺CD29ʰⁱ Cells (%)
8
6
4
2
0
***
Vehicle
CCL19(8-83)
Mammosphere-Forming Efficiency (%)
0.8
0.6
0.4
0.2
0
*
Vehicle
CCL19(8-83)
E
Inject 1µg CCL19(8-83) once a week
Transplant WT+ tumor tissue into inguinal mammary fat pads of 8 week old WT recipients
Weigh tumors and process cells 8 weeks later
Proportion of CD24⁺CD29ʰⁱ Cells (%)
8
6
4
2
0
***
Vehicle
CCL19(8-83)
Mammosphere-Forming Efficiency (%)
2.0
1.5
1.0
0.5
0
*
Vehicle
CCL19(8-83)

SUPPORTING INFORMATION

Supplementary Experimental Procedures

Immunohistochemistry (IHC)

Immunohistochemical analysis was performed using standard procedures. Briefly, antigen retrieval of FFPE mouse mammary sections was carried out by boiling slides in 0.1M sodium citrate buffer (pH 6.0) under pressure. Slides were immersed in 3% hydrogen peroxide in PBS for 20 minutes with gentle agitation to inhibit endogenous peroxidase activity and blocked for 30 minutes in 10% normal serum in PBS to prevent non-specific antibody binding. Slides were then incubated overnight at 4°C with mouse anti-α-smooth muscle actin (α-SMA, Dako). Specific antibody binding was detected using the EnVision Dual Link System (Vector Labs) followed by incubation with diaminobenzidine (DAB) substrate (Dako). Sections were counterstained with haemotoxylin, dehydrated and mounted.

Calcium (Ca^{+}) Signaling Analysis

Intracellular calcium mobilization assay was performed on cells isolated from tumors dissected from C57Bl/6 MMTV-PyMT mice at 20 weeks of age as described (1). Ligands added were CCL21 (100ng/ml) and lysophosphatidic acid (LPA) (50ng/ml).

Enzyme-Linked Immunosorbent Assay (ELISA)

Wells were coated in CCL21 and CCL19 capture antibody (R&D) and receptors blocked using PBS/3%BSA for 1 hour at 37°C. After determining WT and CCR7 KO mammary gland weight, fat pad samples were homogenized in PBS buffer (10% glycerol, 1x protease inhibitor) and aliquotted to coated wells for 90 minutes at 37°C. Detection antibody (R&D) was added for 1 hour then streptavidin-HRP added for 30 minutes.

Proliferation Assay

Isolated lineage-negative mouse mammary cells were plated in adherent culture (DMEM:F12/10% FCS, supplemented with 20ng/ml EGF, 5μg/ml insulin, 0.5μg/ml hydrocortisone, penicillin-streptomycin, and 0.25μg/ml fungazone) in 96-well plates and the following day were serum-starved for 4 hours. The cell proliferation assay was carried out 24 hours later using the XTT Cell Proliferation Kit (ATCC) according to manufacturer's instructions, using 100ng/ml CCL19 and CCL21. FCS was used at a concentration of 5%.

Supplementary References

1. Kochetkova M, Kumar S, McColl SR. Chemokine receptors CXCR4 and CCR7 promote metastasis by preventing anoikis in cancer cells. Cell death and differentiation. 2009;16(5):664-73. Epub 2009/01/13.

SUPPLEMENTARY FIGURES

Supplementary Figure 1 (Related to Figure 1)

(**a**) Serial sections of mouse mammary tissue from normal mice and at different tumourigenic stages stained with haemotoxylin and eosin (H&E) and for α-smooth muscle actin (α-SMA) as indicated. (**b**) Mammary cells were gated to exclude debris, dead cells and doublets (top) and proportions of CCR7-positive cells in mammary epithelial cell preparations from corresponding stages in (a) were analyzed by flow cytometry(bottom). Shaded histograms= fluorescence-minus-one negative gate. wo= weeks old.

Supplementary Figure 2 (Related to Figure 1)

(**a**) Expression of CCR7 ligands (CCL21 and CCL19) in WT and CCR7 KO mammary fat pads with excised inguinal lymph nodes was assessed by ELISA. n=6 glands per genotype. (**b**) Calcium mobilization analysis of PyMT-expressing WT+ mouse mammary cells in response to lysophosphatidic acid (LPA) (positive control) and the CCR7 ligand, CCL21. Arrowheads indicate a point of stimulus addition.

Supplementary Figure 3

Ablation of CCR7 has no effect on early mammary tumourigenesis in MMTV-PyMT mice. (**a**) Top: Representative images of inguinal mammary glands of WT+ (left) and CCR7 KO+ (right) mice harvested at 8 and 11 weeks of age as indicated. Arrowheads indicate areas of epithelial hyperplasia. LN= lymph node. Bottom: Quantitation of area of hyperplasia in WT+ and CCR7 KO+ at 8 weeks old. n=6 glands per genotype. (**b**) Serial sections of mouse mammary tissue from WT+ and CCR7 KO+ mice at 8 weeks old stained with haemotoxylin and eosin (H&E) and for α-smooth muscle actin (α-SMA) as indicated.

Supplementary Figure 4 (Related to Figure 3)

All cells were pre-gated to exclude debris, dead cells and doublets. (**a-b**) Flow cytometry gating strategy for delineating the stem cell-enriched population ($CD24^{+}CD29^{hi}$) and non-stem cell populations ($CD24^{+}CD29^{lo}$ cells and stromal cells) and proportion of CCR7 positive cells within these populations, in normal mice (**a**) and from MMTV-PyMT mice (**b**). (**c**) Flow cytometry gating strategy for delineating the stem cell-enriched population ($CD44^{+}CD24^{-}$) and non-stem cell population ($CD44^{-}CD24^{+}$) in human mammary epithelium, and proportion of CCR7 positive cells within these populations as indicated. (**d-e**) Flow cytometry gating strategy for delineating mouse (**d**) and human (**e**) stem cell-enriched populations based on alternative $CD49f^{+}DLL1^{+}DNER^{+}$ surface marker expression, together with representative plots demonstrating proportion of CCR7 positive cells within these populations. "FMO" and shaded histograms= fluorescence minus one negative gates.

Supplementary Figure 5 (Related to Figure 3)

(**a-b**) CCR7 deletion decreases proportion of the stem cell-enriched population in normal (**a**) and PyMT-expressing mice (**b**) designated by a putative marker profile of Lin^{-} $CD49f^{+}DLL1^{+}DNER^{+}$. Data are representative of at least three independent experiments, n=6 mice per genotype. (**c**) CCR7 stimulation does not have any effect on proliferation of WT+ mammary cells in adherent culture. Shown are results of XTT proliferation assay with and without addition of CCR7 ligands. FCS was used as a positive control. (**d**) The stimulatory effect of CCL19 and CCL21 on MFE of MMTV-PyMT cells is dependent on CCR7. The primary MFE of CCR7 KO+ (n=4 mice) mouse mammary cells was not affected by the addition of these chemokines. (**e**) Effect of stimulation of primary WT+ (n=6 mice) mammosphere culture with chemokine ligands for receptors CCR6, CXCR3, CXCR4 and CXCR5 respectively.

Supplementary Figure 6 (Related to Figure 4)

Representative images of WT recipient glands engrafted with WT+ or CCR7 KO+ mammosphere-derived cells as indicated. Shown are contralateral glands in which both WT+ and CCR7 KO+ cells produced outgrowths (black arrowheads), to demonstrate differences in size between lesions. At the lowest dilution, only WT+ cells produced any outgrowth. LN= lymph node**.**

Supplementary Figure 7 (Related to Figure 6)

(**a**) Total mammary epithelial cell count in MMTV-PyMT mice following injection with vehicle or $CCL19_{(8\text{-}83)}$ antagonist for 8 weeks in contralateral inguinal mammary fat pads. (**b**) Weight of mammary glands. (**c**) Comparison of stem cell-enriched population in MMTV-PyMT glands delineated by alternative marker set $Lin^-CD49f^+DLL1^+DNER^+$. (**d**) Treatment of mammary glands with vehicle control (left) or $CCL19_{(8\text{-}83)}$ (right) does not alter CCR7 expression levels in the $Lin^-CD24^+CD29^{hi}$ population. Shaded histograms = fluorescence minus one negative gates. (**e**) Treatment with $CCL19_{(8\text{-}83)}$ does not change cellularity of transplanted tumor tissue despite affecting the stem cell-like pool. (**f**) Comparison of the stem cell-enriched population in transplanted glands treated with $CCL19_{(8\text{-}83)}$ or vehicle, as delineated by alternative marker set $Lin^-CD49f^+DLL1^+DNER^+$.

Supplementary Figure 1

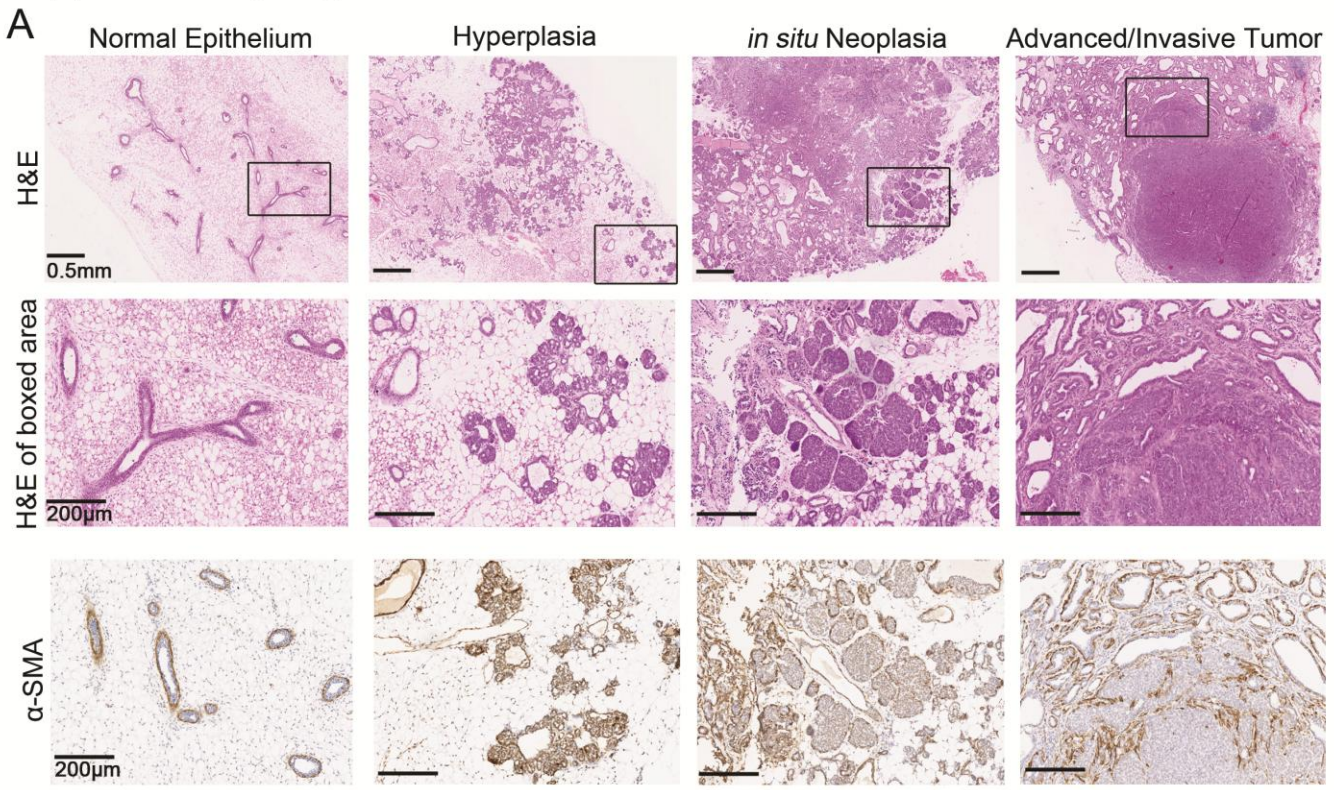

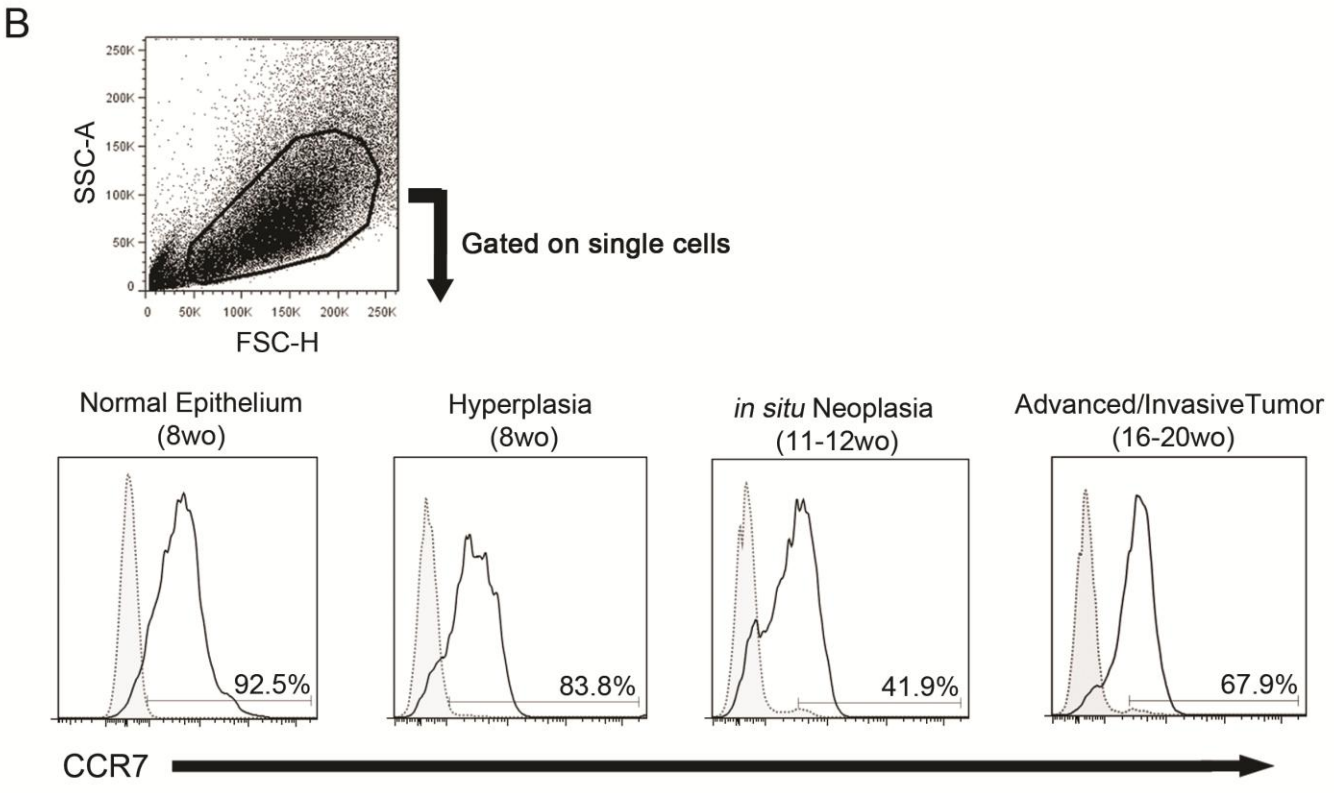

Supplementary Figure 2

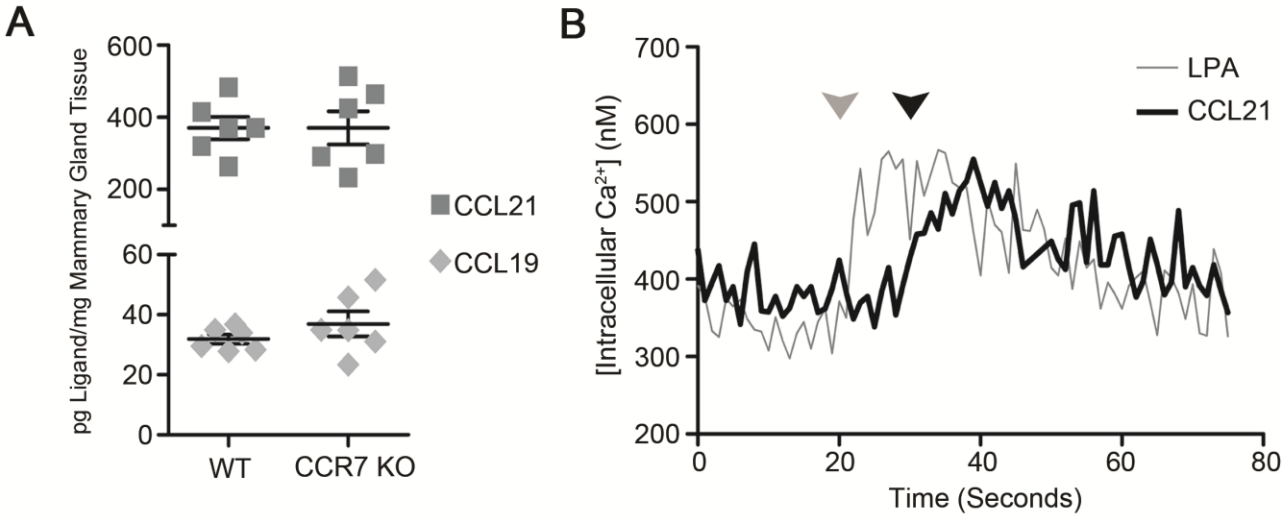

Supplementary Figure 3

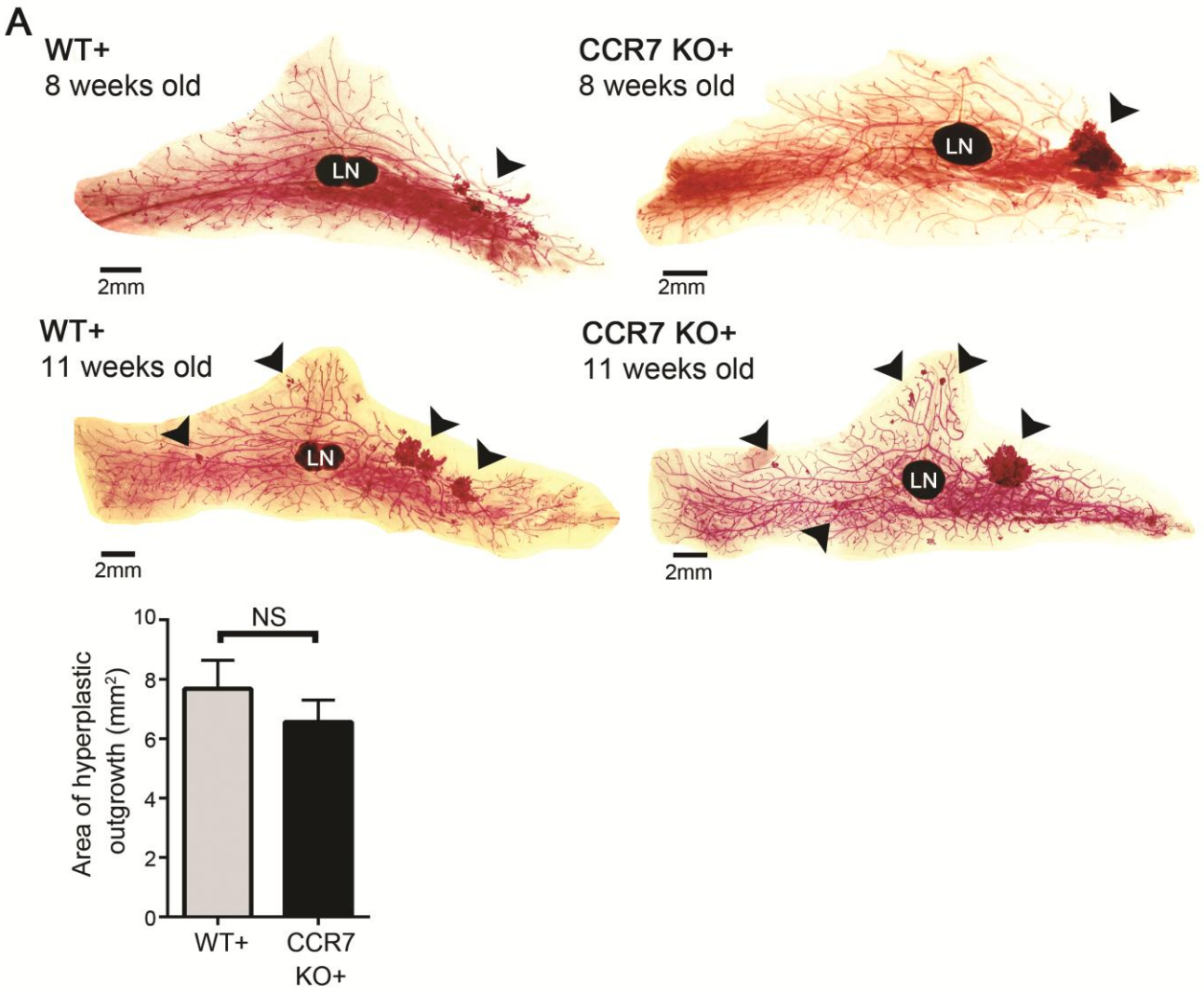

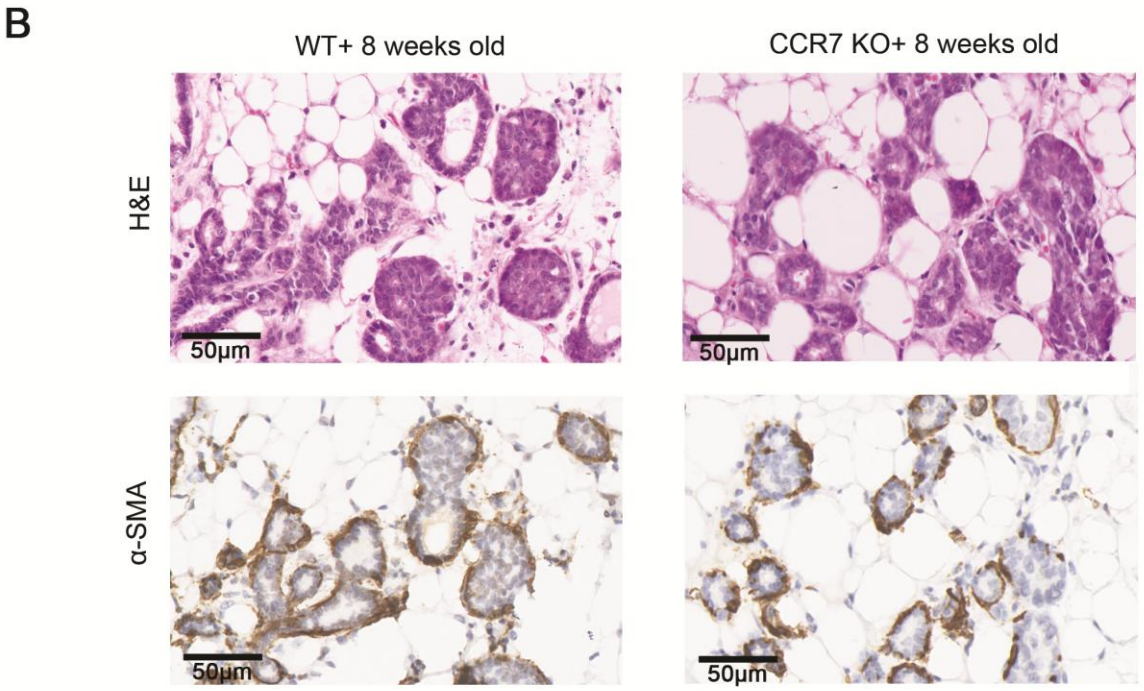

Supplementary Figure 4

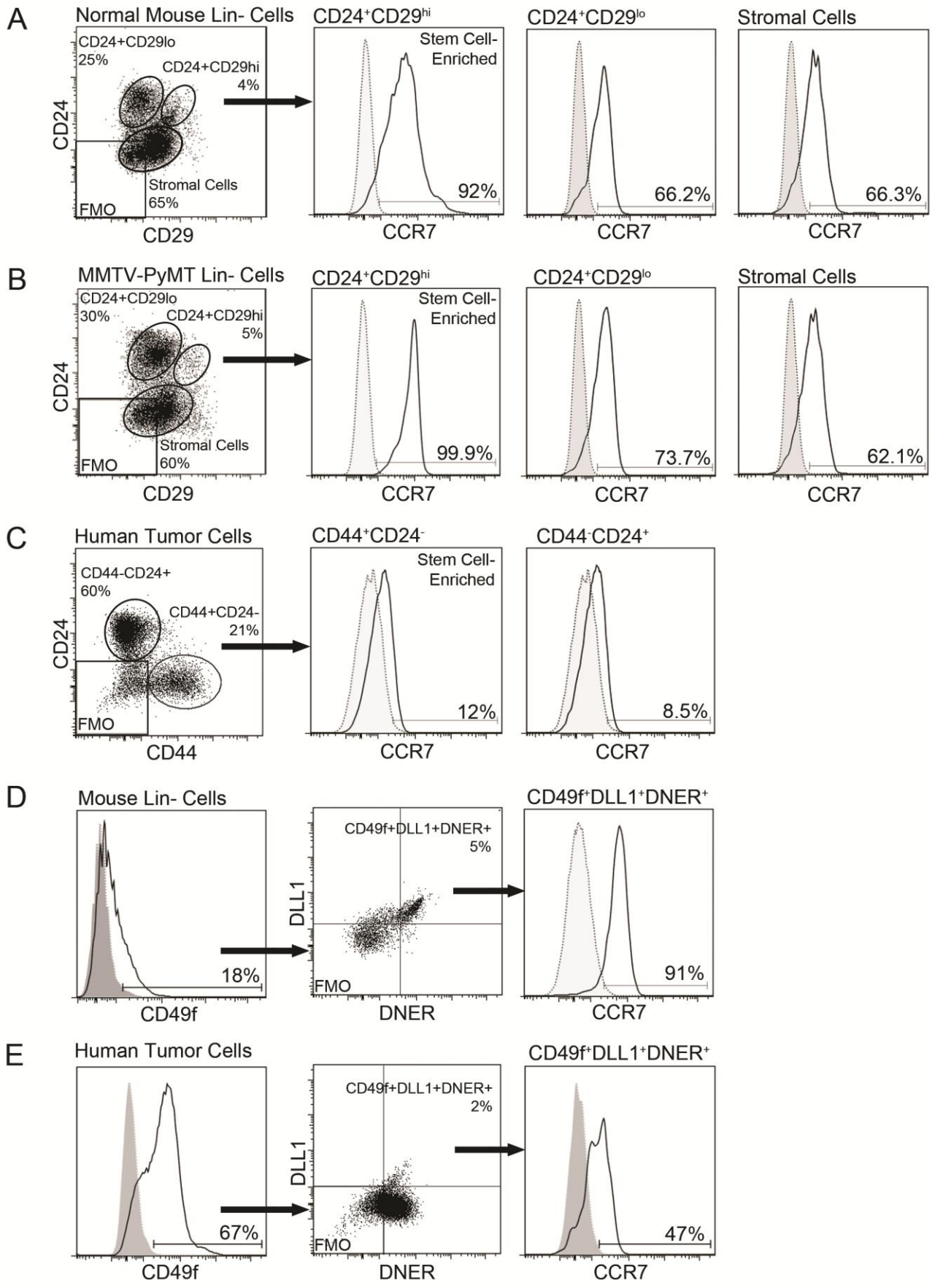

Supplementary Figure 5

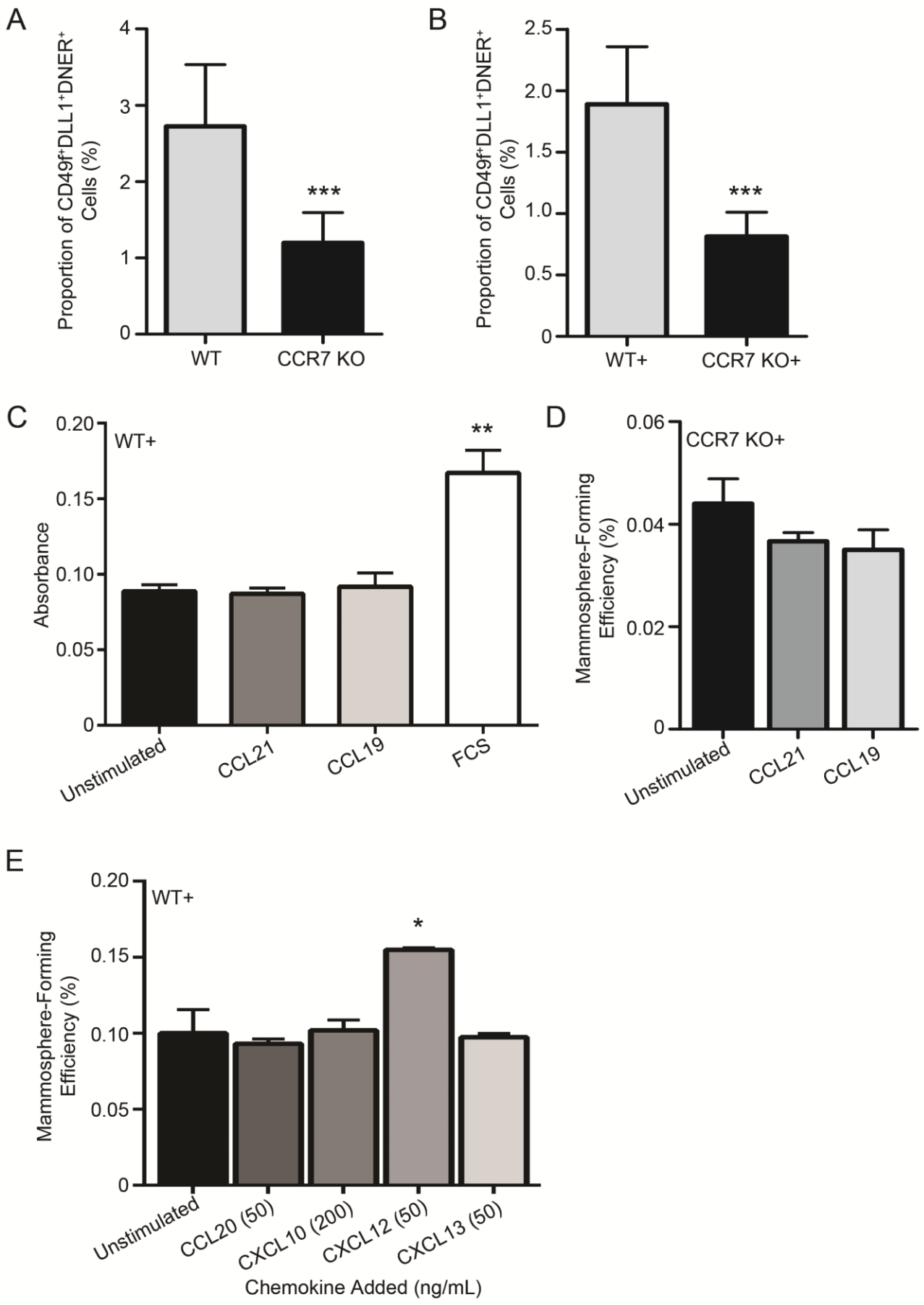

Supplementary Figure 6

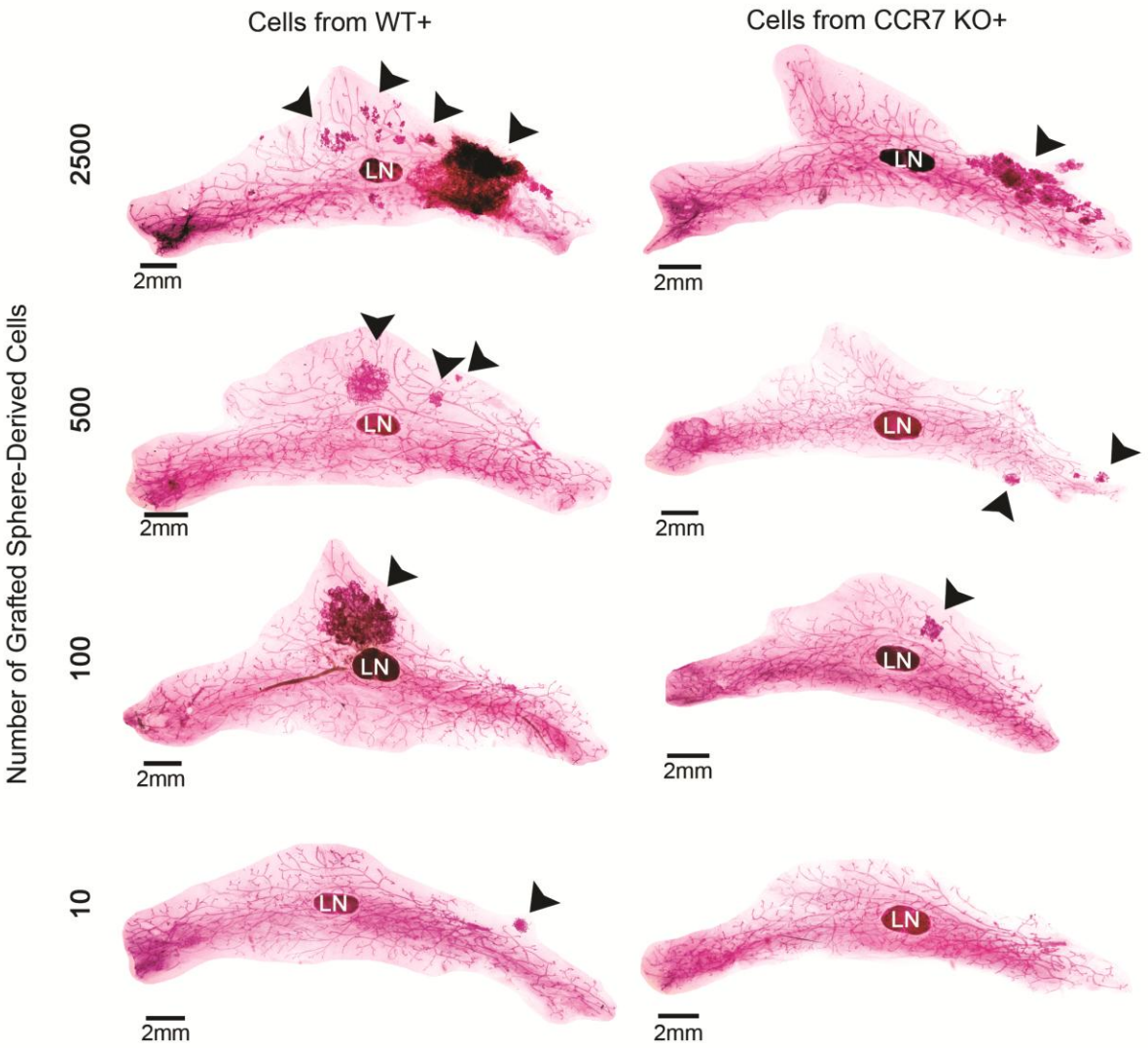

Supplementary Figure 7